Asian Journal of Chemistry; Vol. 36, No. 9 (2024), 2097-2114

ASIAN JOURNAL OF CHEMISTRY

https://doi.org/10.14233/ajchem.2024.32117

Ecofriendly Synthesis, Spectroscopic Analysis and *in silico* Study of Coumarin Hydrazide-Hydrazone Derivative Targeted against HIV and SARS-CoV-2

SHIPRA GAUTAM[1], POONAM RAWAT[1,*], PRAKASH[1], ANANT RAM[1], AMUL DARWARI[1], SHARDA PANDEY[2], ANUPAMA PANDEY[1] and R.N. SINGH[1,*]

[1]Department of Chemistry, University of Lucknow, Lucknow-226007, India
[2]Department of Physics, University of Lucknow, Lucknow-226007, India

*Corresponding authors: E-mail: prchem.rawat@gmail.com; rnsvk.chemistry@gmail.com

Received: 10 June 2024; *Accepted*: 25 July 2024; *Published online*: 30 August 2024; AJC-21736

Coumarin based hydrazide-hydrazone (CHH) derivative was synthesized and evaluated for *in silico* antiviral activity against SARS-CoV-2 and anti-HIV activity. The experimental techniques (FT-IR, ^{1}H NMR, ^{13}C NMR and UV-vis) and computational calculations (B3LYP functional and 6-31G(d,p)/6-311G(d,p) level of theory) were used for the detailed analysis of the synthesized compound. By following the mechanosynthesis methodology, the excellent yield and reduction in reaction time were observed in the grinding method when compared to conventional method. The rotational barrier between conformer I and II of CHH was found to be 5.102 Kcal/mol in the gas phase. The FT-IR spectrum was carried out to support the hydrogen bonding pattern proposed by reported crystalline structure. The electronic descriptors studies indicate CHH used as useful synthon for new heterocyclic compounds. The first static hyperpolarizability (β_0) of the CHH was calculated as 17.47 and 25.93 10^{-30} esu at B3LYP/6-31G (d,p) and B3LYP/6-311G(d,p) basis set indicates CHH may be used as non-linear optical material. The ADMET, isoelectronic molecular electrostatic potential surfaces (MEPS), NBO and QTAIM studies were also performed. According to molecular docking, the synthesized CHH compound showed strong antiviral efficacy against SARS COV-2 major protein (M^{pro}) with PDB code 6lu7 and anti-HIV antibody DH501, an unmutated common ancestor with PDB ID 6p3b.

Keywords: Coumarin, Hydrazide-hydrazone, Mechanosynthesis, Antiviral activity, ADMET, QTAIM.

INTRODUCTION

Several antiviral chemotherapy therapies make use of synthetic and semisynthetic drugs derived from natural sources, which have proven to be an excellent source of molecules with antiviral properties [1]. Till today, more than 1300 different coumarin derivatives have been identified which show a wide spectrum of biological activities [2]. Viruses can cause wide range of diseases and have been viewed as a serious danger to both human health and the global economy [3]. Various natural, semi-synthetic and synthetic coumarin phytochemicals have the tendency to inhibit virus activity, after chemical modification in the structure [4-12]. Chemically modified coumarins have great potential as drugs for the treatment of various viral diseases [13,14].

Nowadays, DFT calculations have been integrated to take advantage of inter atomic potentials for searching property prediction of the compounds. The ADMET characteristic of any pharmacokinetic moiety can be studied more effectively with computational techniques. Predicting the future course of a drugs and the physiological impacts it induces, such as the extent of oral absorption and gastrointestinal absorption, is an essential component of drug development. Thus, ADMET study is one of the most essential parts of computational drug design [15]. Over the past four years, scientists have intensified their research efforts to uncover novel medications and vaccines to battle the COVID-19 pandemic. In this context, the crystalline structure of SARS-CoV-2 main protease (M^{pro}) is considered as a target to discover therapeutic agents to COVID-19 since COVID-19 pandemic has resulted in several hundred thousand deaths, presenting an unparalleled risk to public health [9]. In addition, by investigating the potential contacts and energies needed to block the activity of M^{pro}, molecular docking calculations provide a useful tool for predicting the inhibitory activity of organic molecules towards M^{pro}.

Due to the variety of applications in the food industry, cosmetics, medicine and pharmacology, coumarin derivatives are the subject of ongoing study into their synthesis. Therefore, high demands for their synthesis often result in an increased generation of different waste chemicals. In order to minimize the utilization and generation of toxic organic substances, green synthetic methods are applied in this manner. These methods are getting more attention in the last few decades [16]. A wide range of techniques are covered by the green chemistry methodology, such as the use of microwaves, ultrasonic waves, ionic liquids, deep eutectic solvents, solvent-free synthesis, mechanosynthesis and multicomponent reactions. These environmental friendly synthetic techniques have effectively completed all common condensation processes for coumarin synthesis, such as the Knoevenagel, Perkin, Kostanecki-Robinson, Pechmann and Reformatsky reactions [17].

Due to the growing demand for coumarin derivatives in the pharmaceutical business, efforts are being made to simplify the synthetic strategies of important building blocks and provide comprehensive information on their spectrum analysis, structural elucidation, and chemical reactivity. Coumarin possesses a distinctive structural characteristic, namely its remarkable simplicity of assembly and modification with inexpensive and readily accessible starting components. Therefore, the main aim of this research is to report green, simple and low-cost protocol for the synthesis of coumarin based hydrazone derivative (CHH) in the presence of acetic acid as an efficient, relatively non-toxic and inexpensive catalyst. The synthesized CHH has been fully structurally characterized by modern spectroscopic techniques. Theoretical investigations of the structure, isoelectronic molecular electrostatic potential surfaces, NBO, NLO, QTAIM have been performed using DFT approach. Apart of this, a detailed spectroscopic characterizations, global electronic parameters, ADMET and molecular modeling targeted against SARS-CoV-2 and HIV have also been performed. This work is important as it theoretically explores and identifies the binding affinities and interactions of CHH on energy basis and correlates the spectral data in detail.

EXPERIMENTAL

Conventional/traditional method for the synthesis of CHH: To a boiling solution of 3-acetylcoumarin (5 mmol) in 25 mL ethanol, added *p*-toluene sulfonyl hydrazide (5 mmol, 20 mL ethanol) dropwise over a period of 10 min in the presence of acetic acid as catalyst. The reaction mixture was refluxed for 4 h at 100 ºC and allowed to cool overnight. The completion of the reaction was checked by TLC. The crude product was filtered and dried at reduced pressure. The crude product was purified by column chromatography. Colour: light yellow; yield: 62%; m.w.: 356.40, m.p.: 223 ºC, Elemental analysis of m.f.: $C_{18}H_{16}N_2O_4S$, calcd. (found) %: C, 60.66 (60.62); H, 4.53 (4.53); N, 7.86 (7.82).

Green synthesis or mechanosynthesis of coumarin based hydrazide-hydrazone (CHH) derivative: The mixture of 3-acetyl coumarin (5 mmol) and *p*-toluene sulfonylhydrazide (5 mmol) were grinded together in the mortar pestle using acetic acid as catalyst (1 drop). After 0.5 h, the colour of material gradually changed from off white to light yellow (**Scheme-I**). The formed product was purified by recrystallization. Colour: light yellow; yield: 95%; m.w.: 356.40, m.p.: 220-222 ºC, Elemental analysis of $C_{18}H_{16}N_2O_4S$, calcd. (found) %: C, 60.66 (60.60); H, 4.53 (4.50); N, 73.86 (7.81).

Quantum chemical calculations: Gaussian 09 software package [18] was utilized to predict the molecular structure, FT-IR, ^{1}H NMR, ^{13}C NMR, TD-DFT, thermochemistry, QTAIM, NBO, NLO and global descriptors of CHH at B3LYP/6–31G-(d,p) and B3LYP/6–311G(d,p), basis set [19-22]. ^{1}H and ^{13}C NMR chemical shifts have been determined by applying the

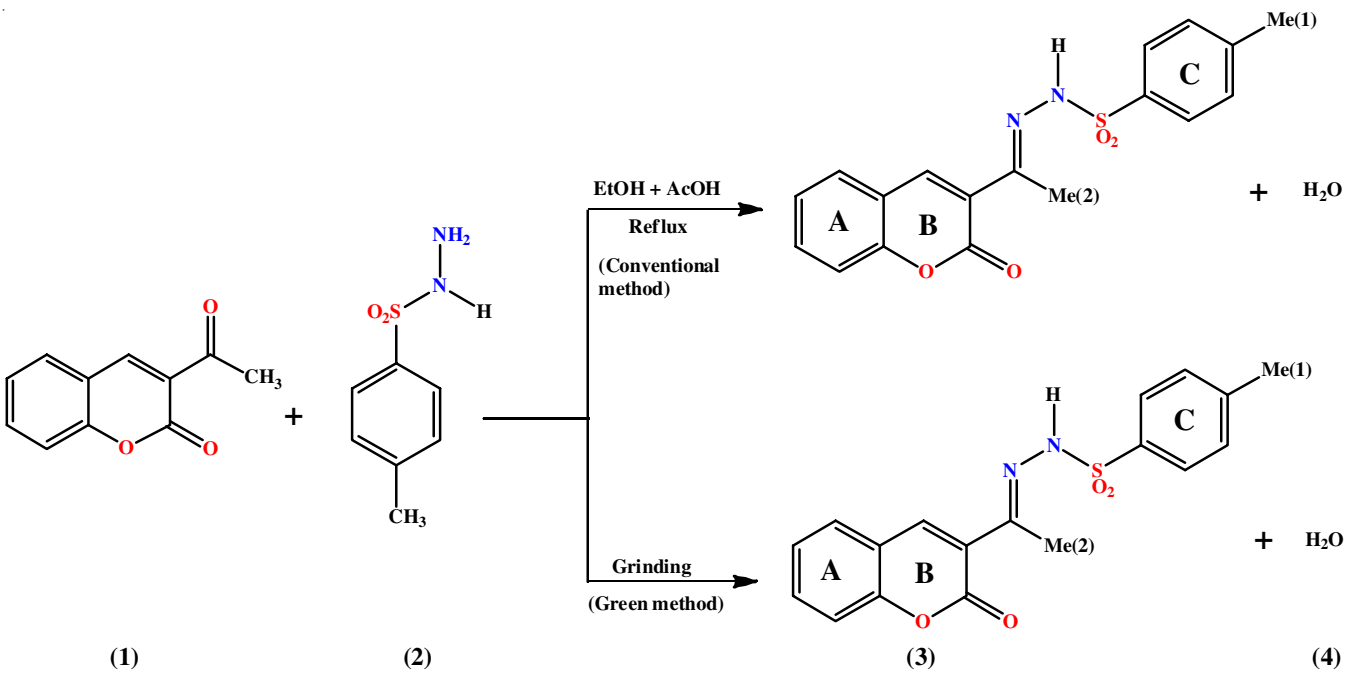

Scheme-I: Schematic representation for the synthesis of CHH (**3**) by conventional and grinding method

gauge including atomic orbital (GIAO) technique. The solvent effects on the spectrum (^{1}H, ^{13}C NMR, TD-DFT) of CHH molecule was also studied using IEFPCM model (DMSO solvent). The assignments of FT-IR wavenumbers was done by using Gar2ped programme [23].

RESULTS AND DISCUSSION

The schematic formation of coumarin based hydrazide-hydrazone (CHH) derivative (**3**) by conventional and grinding method is shown in **Scheme-I**. In the conventional method, both the equimolar reactants were mixed together in ethanol solvent in the presence of acetic acid as catalyst and then refluxed for 4 h at 100 ºC. The formed precipitate was further purified by column chromatography. The product obtained in moderate yield (62%).

In green protocol, grinding method has been used which is appealing ecofriendly technique for efficient organic synthesis with several advantages, such as: mild reaction condition, easy separation and purifications, high efficiency and selectivity and environmental acceptability. The equimolar amount of 3-acetylcoumarin (**1**) and *p*-toluene sulfonyl hydrazide (**2**) were grinded together in the mortar pestle using acetic acid as catalyst at room temperature and 95% yield was obtained within 0.5 h. In the conventional method when the temperature was elevated from room temperature to 100 ºC, but the yield was somewhat low in comparison to the mechanosynthesis (grinding process).

The initial geometry for optimization has been taken from the single crystal data [24] of the investigated CHH molecule. The molecular optimization and conformational studies of CHH have been conducted without imposing any symmetry constrains on the molecule. Single crystal structure determination showed that CHH crystallizes into a monoclinic form having eight molecules per unit cells (Z = 8). The orthorhombic system belongs to a space group $P2_1/n$, with a = 11.680 (3) Å, b = 15.450 (3) Å, c = 17.890 (4) Å and $\alpha = \gamma = \beta = 90°$ (3). The rotational energy barrier difference between conformer I and II has been found to be 5.102 Kcal/mol since the conformer I and II has the energy of -1504.350569 and -1504.358704 a.u. The conformational search has been done around the dihedral angle (C8–C9–C11–N12) of the inves-tigated CHH molecule. The dihedral angle value of conformer I and II was found -22.41604º and 144.45325º, respectively. The optimized geometries of CHH conformer I and II is given in Fig. 1 and calculated geometrical bond lengths, bond angles and dihedral angles are given in Table-1. Both conformers show the C1 point group, however, Conformer I is more stable than conformer II due to its lower energy. Due to change in the conformation, charges and bond length of particular atoms are also changed. The bond length of C11-C15 and C15-H32 of methyl group situated at azomethine carbon atom are longer in conformer I because C15-H32 involve in H-H bonding with N-H.

The results of the calculation of thermochemistry for synthesized CHH at B3LYP/6-311g (d,p) at 25 ºC are listed in Table-2. It should be mentioned that the net spontaneity of a chemical reaction is determined by the Gibbs free energy change of reaction (ΔG). The reaction was spontaneous at 25 ºC, as indicated by the determined negative value of (ΔG) for the studied reaction. The temperature of the reaction must reach 100 ºC in order for the complete conversion of the reactants into product.

Quantum theory of atoms in molecules (QTAIMs) and weaker interactions analysis: QTAIMs theory is helpful for calculating the bond strength, which is expressed as an increase or decrease in the electron density at the bond critical point (ρ_{BCP}). The electron densities between the atoms depend on the nature of the bonded atoms. In shared (covalent) bonding, the value of Laplacian of electron density should be greater than zero ($\nabla^2\rho_{BCP} > 0$ a.u.) and for closed-shell interaction (ionic, van der Waals, hydrogen, dihydrogen, H-H bonding and other weak interactions), the value of Laplacian of electron density should be less than 0.10 a.u. [18]. Various interactions are classified on the basis of geometrical (bond length, bond angle), topological and energetic parameters in QTAIMs. In this work, hydrogen-hydrogen (H-H) and oxygen-nitrogen (O-N) interaction have been calculated by applying the Bader's theory of atom in molecules. Molecular graph of CHH is shown in Fig. 2. Geometrical parameters for intramolecular interactions, sum of van der Waal radii of interacting atoms and topological parameters are given in Table-3. Various types of interactions have been visualized in the molecular graph of the synthesized CHH molecule and are classified on the basis of geometrical, topological and energetic parameters such as (i) hydrogen-hydrogen van der Waal interaction (C13–H31···H38–C21/C21–H38···H31–C13) due to ($\nabla^2\rho_{BCP}$) > 0, $H_{BCP} > 0$ and $d_{H\cdots O} < (r_H + r_O)$ and (ii) van der Waal interaction (C10–H30···H32–

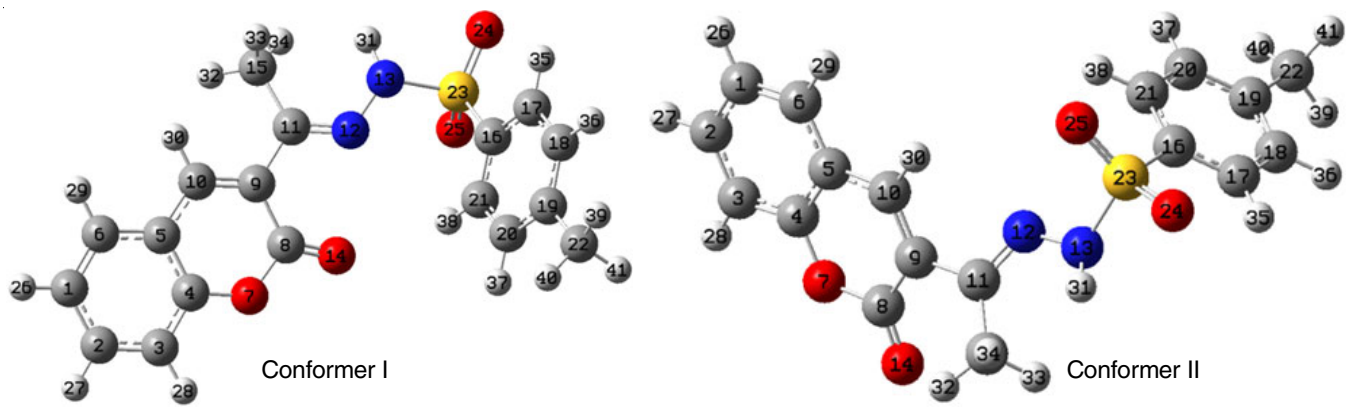

Fig. 1. Optimized geometry of coumarin based hydrazide-hydrazone (CHH) derivative for conformer I and II

TABLE-1
SELECTED OPTIMIZED GEOMETRICAL PARAMETERS OF CHH CONFORMER I AND II USING B3LYP/6-311G(d,p) [BOND LENGTH (Å), BOND ANGLE (°) AND DIHEDRAL ANGLE (°)]

Bond length (Å)		Bond angle (°)		Dihedral angle (°)	
		Conformer I			
R(1,2)	1.4043	A(2,1,6)	119.8980	D(6,1,2,3)	0.03120
R(1,6)	1.3867	A(2,1,26)	119.9879	D(6,1,2,27)	-179.9658
R(1,26)	1.0850	A(6,1,26)	120.1141	D(26,1,2,3)	-179.9686
R(2,3)	1.3907	A(1,2,3)	120.7950	D(26,1,2,27)	0.0344
R(2,27)	1.0856	A(1,2,27)	119.8089	D(2,1,6,5)	0.0597
R(3,4)	1.3959	A(3,2,27)	119.3961	D(2,1,6,29)	-179.9450
R(3,28)	1.0843	A(2,3,4)	118.8352	D(26,1,6,5)	-179.9405
R(4,5)	1.4049	A(2,3,28)	122.0202	D(26,1,6,29)	0.0548
R(4,7)	1.3602	A(4,3,28)	119.1446	D(1,2,3,4)	-0.0684
R(5,6)	1.4091	A(3,4,5)	121.5021	D(1,2,3,28)	179.9880
R(5,10)	1.4340	A(3,4,7)	117.9490	D(27,2,3,4)	179.9286
R(6,29)	1.0865	A(5,4,7)	120.5489	D(27,2,3,28)	-0.0149
R(7,8)	1.3998	A(4,5,6)	118.5163	D(2,3,4,5)	0.0158
R(8,9)	1.4849	A(4,5,10)	117.3683	D(2,3,4,7)	-179.9481
R(8,14)	1.2041	A(6,5,10)	124.1136	D(28,3,4,5)	179.9610
R(9,10)	1.3656	A(1,6,5)	120.4532	D(28,3,4,7)	-0.0029
R(9,11)	1.4796	A(1,6,29)	120.5883	D(3,4,5,6)	0.0723
R(10,30)	1.0859	A(5,6,29)	118.9585	D(3,4,5,10)	179.6166
R(11,12)	1.2902	A(4,7,8)	124.2830	D(7,4,5,6)	-179.9647
R(11,15)	1.5145	A(7,8,9)	116.0104	D(7,4,5,10)	-0.4204
R(12,13)	1.3558	A(7,8,14)	116.0169	D(3,4,7,8)	179.8348
R(13,23)	1.7367	A(9,8,14)	127.9660	D(5,4,7,8)	-0.1295
R(13,31)	1.0244	A(8,9,10)	118.7996	D(4,5,6,1)	-0.1098
R(15,32)	1.0901	A(8,9,11)	120.0882	D(4,5,6,29)	179.8948
R(15,33)	1.0969	A(10,9,11)	121.1114	D(10,5,6,1)	-179.6210
R(15,34)	1.0965	A(5,10,9)	122.9809	D(10,5,6,29)	0.3836
R(16,17)	1.3944	A(5,10,30)	117.1592	D(4,5,10,9)	0.1624
R(16,21)	1.3980	A(9,10,30)	119.8471	D(4,5,10,30)	-178.5306
R(16,23)	1.7817	A(9,11,12)	117.2947	D(6,5,10,9)	179.6788
R(17,18)	1.3935	A(9,11,15)	119.5377	D(6,5,10,30)	0.9857
R(17,35)	1.0842	A(12,11,15)	123.1335	D(4,7,8,9)	0.8730
R(18,19)	1.4012	A(11,12,13)	120.2723	D(4,7,8,14)	-178.2581
R(18,36)	1.0866	A(12,13,23)	114.2464	D(7,8,9,10)	-1.0780
R(19,20)	1.4035	A(12,13,31)	120.4716	D(7,8,9,11)	178.5974
R(19,22)	1.5095	A(23,13,31)	109.1754	D(14,8,9,10)	177.9315
R(20,21)	1.3920	A(11,15,32)	111.9170	D(14,8,9,11)	-2.3931
R(20,37)	1.0866	A(11,15,33)	111.9060	D(8,9,10,5)	0.5966
R(21,38)	1.0841	A(11,15,34)	110.5263	D(8,9,10,30)	179.2559
R(22,39)	1.0934	A(32,15,33)	108.4087	D(11,9,10,5)	-179.0754
R(22,40)	1.0943	A(32,15,34)	106.4617	D(11,9,10,30)	-0.4161
R(22,41)	1.0969	A(33,15,34)	107.3654	D(8,9,11,12)	-22.7673
R(23,24)	1.4660	A(17,16,21)	121.7605	D(8,9,11,15)	159.2907
R(23,25)	1.4623	A(17,16,23)	118.5944	D(10,9,11,12)	156.9005
		A(21,16,23)	119.6306	D(10,9,11,15)	-21.0415
		A(16,17,18)	118.7759	D(9,11,12,13)	-174.2327
		A(16,17,35)	119.8653	D(15,11,12,13)	3.6290
		A(18,17,35)	121.3574	D(9,11,15,32)	-21.2392
		A(17,18,19)	121.0614	D(9,11,15,33)	100.6767
		A(17,18,36)	119.3848	D(9,11,15,34)	-139.7157
		A(19,18,36)	119.5538	D(12,11,15,32)	160.9449
		A(18,19,20)	118.6242	D(12,11,15,33)	-77.1392
		A(18,19,22)	120.8314	D(12,11,15,34)	42.4684
		A(20,19,22)	120.5354	D(11,12,13,23)	-152.9361
		A(19,20,21)	121.4475	D(11,12,13,31)	-19.8600
		A(19,20,37)	119.5126	D(12,13,23,16)	-65.6604
		A(21,20,37)	119.0399	D(12,13,23,24)	179.9150
		A(16,21,20)	118.3272	D(12,13,23,25)	50.0601
		A(16,21,38)	120.6059	D(31,13,23,16)	156.1402
		A(20,21,38)	121.0492	D(31,13,23,24)	41.7156
		A(19,22,39)	111.5445	D(31,13,23,25)	-88.1393
		A(19,22,40)	111.3994	D(21,16,17,18)	0.1198
		A(19,22,41)	110.8930	D(21,16,17,35)	179.6945
		A(39,22,40)	108.2038	D(23,16,17,18)	-178.4891

		A(39,22,41)	107.4631	D(23,16,17,35)	1.0856
		A(40,22,41)	107.1386	D(17,16,21,20)	0.3388
		A(13,23,16)	102.3126	D(17,16,21,38)	178.8255
		A(13,23,24)	102.3008	D(23,16,21,20)	178.9336
		A(13,23,25)	109.9760	D(23,16,21,38)	-2.5798
		A(16,23,24)	110.4432	D(17,16,23,13)	-103.5771
		A(16,23,25)	109.0043	D(17,16,23,24)	4.7279
		A(24,23,25)	121.0430	D(17,16,23,25)	139.9995
				D(21,16,23,13)	77.7836
				D(21,16,23,24)	-173.9113
				D(21,16,23,25)	-38.6397
				D(16,17,18,19)	-0.2513
				D(16,17,18,36)	179.7109
				D(35,17,18,19)	-179.8194
				D(35,17,18,36)	0.1428
				D(17,18,19,20)	-0.0780
				D(17,18,19,22)	178.8356
				D(36,18,19,20)	179.9600
				D(36,18,19,22)	-1.1265
				D(18,19,20,21)	0.5563
				D(18,19,20,37)	-179.4861
				D(22,19,20,21)	-178.3605
				D(22,19,20,37)	1.5970
				D(18,19,22,39)	20.8074
				D(18,19,22,40)	141.8351
				D(18,19,22,41)	-98.9314
				D(20,19,22,39)	-160.2998
				D(20,19,22,40)	-39.2721
				D(20,19,22,41)	79.9614
				D(19,20,21,16)	-0.6814
				D(19,20,21,38)	-179.1611
				D(37,20,21,16)	179.3609
				D(37,20,21,38)	0.8813
Conformer II					
R(1,2)	1.4019	A(2,1,6)	119.8642	D(6,1,2,3)	0.0052
R(1,6)	1.3840	A(2,1,26)	119.9774	D(6,1,2,27)	-179.9666
R(1,26)	1.0832	A(6,1,26)	120.1584	D(26,1,2,3)	-179.978
R(2,3)	1.3880	A(1,2,3)	120.7797	D(26,1,2,27)	0.0502
R(2,27)	1.0838	A(1,2,27)	119.8170	D(2,1,6,5)	0.0827
R(3,4)	1.3937	A(3,2,27)	119.4034	D(2,1,6,29)	-179.9441
R(3,28)	1.0826	A(2,3,4)	118.9357	D(26,1,6,5)	-179.9341
R(4,5)	1.4022	A(2,3,28)	122.0301	D(26,1,6,29)	0.0391
R(4,7)	1.3579	A(4,3,28)	119.0342	D(1,2,3,4)	-0.0416
R(5,6)	1.4073	A(3,4,5)	121.3883	D(1,2,3,28)	179.9983
R(5,10)	1.4326	A(3,4,7)	118.0710	D(27,2,3,4)	179.9304
R(6,29)	1.0847	A(5,4,7)	120.5406	D(27,2,3,28)	-0.0298
R(7,8)	1.4026	A(4,5,6)	118.5650	D(2,3,4,5)	-0.0097
R(8,9)	1.4845	A(4,5,10)	117.3644	D(2,3,4,7)	-179.905
R(8,14)	1.1959	A(6,5,10)	124.0682	D(28,3,4,5)	179.9517
R(9,10)	1.3624	A(1,6,5)	120.4669	D(28,3,4,7)	0.0564
R(9,11)	1.4791	A(1,6,29)	120.5235	D(3,4,5,6)	0.0949
R(10,30)	1.0842	A(5,6,29)	119.0096	D(3,4,5,10)	179.5656
R(11,12)	1.2858	A(4,7,8)	124.3910	D(7,4,5,6)	179.9877
R(11,15)	1.5129	A(7,8,9)	115.7302	D(7,4,5,10)	-0.5416
R(12,13)	1.3524	A(7,8,14)	116.1021	D(3,4,7,8)	179.7269
R(13,23)	1.7339	A(9,8,14)	128.1623	D(5,4,7,8)	-0.1693
R(13,31)	1.0221	A(8,9,10)	118.8886	D(4,5,6,1)	-0.1311
R(15,32)	1.0883	A(8,9,11)	119.9942	D(4,5,6,29)	179.8952
R(15,33)	1.0955	A(10,9,11)	121.1160	D(10,5,6,1)	-179.5637
R(15,34)	1.0948	A(5,10,9)	123.0703	D(10,5,6,29)	0.4627
R(16,17)	1.3914	A(5,10,30)	117.1103	D(4,5,10,9)	0.2048
R(16,21)	1.3948	A(9,10,30)	119.8067	D(4,5,10,30)	-178.4951
R(16,23)	1.7838	A(9,11,12)	117.3366	D(6,5,10,9)	179.6436
R(17,18)	1.3913	A(9,11,15)	119.6229	D(6,5,10,30)	0.9437
R(17,35)	1.0825	A(12,11,15)	123.0086	D(4,7,8,9)	1.1301
R(18,19)	1.3988	A(11,12,13)	120.5180	D(4,7,8,14)	-178.0989
R(18,36)	1.0847	A(12,13,23)	114.4689	D(7,8,9,10)	-1.3979
R(19,20)	1.4010	A(12,13,31)	120.6720	D(7,8,9,11)	178.2208

R(19,22)	1.5085	A(23,13,31)	109.6959	D(14,8,9,10)	177.7215
R(20,21)	1.3895	A(11,15,32)	112.0569	D(14,8,9,11)	-2.6598
R(20,37)	1.0848	A(11,15,33)	111.7533	D(8,9,10,5)	0.7813
R(21,38)	1.0822	A(11,15,34)	110.4149	D(8,9,10,30)	179.4476
R(22,39)	1.0917	A(32,15,33)	108.4136	D(11,9,10,5)	-178.833
R(22,40)	1.0928	A(32,15,34)	106.4939	D(11,9,10,30)	-0.1667
R(22,41)	1.0952	A(33,15,34)	107.4618	D(8,9,11,12)	180.000
R(23,24)	1.4595	A(17,16,21)	121.8014	D(8,9,11,15)	1.9918
R(23,25)	1.4552	A(17,16,23)	118.7026	D(10,9,11,12)	-0.3900
		A(21,16,23)	119.4890	D(10,9,11,15)	-178.3981
		A(16,17,18)	118.7362	D(9,11,12,13)	-174.3092
		A(16,17,35)	119.9337	D(15,11,12,13)	3.6260
		A(18,17,35)	121.3262	D(9,11,15,32)	-20.9721
		A(17,18,19)	121.0734	D(9,11,15,33)	100.9407
		A(17,18,36)	119.3149	D(9,11,15,34)	-139.5053
		A(19,18,36)	119.6117	D(12,11,15,32)	161.1379
		A(18,19,20)	118.6187	D(12,11,15,33)	-76.9493
		A(18,19,22)	120.8654	D(12,11,15,34)	42.6047
		A(20,19,22)	120.5073	D(11,12,13,23)	-153.7302
		A(19,20,21)	121.4132	D(11,12,13,31)	-19.2700
		A(19,20,37)	119.6121	D(12,13,23,16)	-65.7072
		A(21,20,37)	118.9747	D(12,13,23,24)	179.9507
		A(16,21,20)	118.3534	D(12,13,23,25)	49.956
		A(16,21,38)	120.5802	D(31,13,23,16)	154.988
		A(20,21,38)	121.0491	D(31,13,23,24)	40.6459
		A(19,22,39)	111.4955	D(31,13,23,25)	-89.3488
		A(19,22,40)	111.3175	D(21,16,17,18)	0.4156
		A(19,22,41)	110.7304	D(21,16,17,35)	179.7023
		A(39,22,40)	108.2365	D(23,16,17,18)	-178.6141
		A(39,22,41)	107.6132	D(23,16,17,35)	0.6726
		A(40,22,41)	107.2677	D(17,16,21,20)	0.0751
		A(13,23,16)	102.0359	D(17,16,21,38)	178.5769
		A(13,23,24)	102.3039	D(23,16,21,20)	179.0973
		A(13,23,25)	110.0217	D(23,16,21,38)	-2.4008
		A(16,23,24)	110.4523	D(17,16,23,13)	-100.8393
		A(16,23,25)	109.0606	D(17,16,23,24)	7.3441
		A(24,23,25)	121.1340	D(17,16,23,25)	142.7984
				D(21,16,23,13)	80.1081
				D(21,16,23,24)	-171.7085
				D(21,16,23,25)	-36.2542
				D(16,17,18,19)	-0.4316
				D(16,17,18,36)	179.5429
				D(35,17,18,19)	-179.7081
				D(35,17,18,36)	0.2665
				D(17,18,19,20)	-0.0374
				D(17,18,19,22)	178.9084
				D(36,18,19,20)	179.9881
				D(36,18,19,22)	-1.0661
				D(18,19,20,21)	0.5476
				D(18,19,20,37)	-179.3738
				D(22,19,20,21)	-178.4021
				D(22,19,20,37)	1.6765
				D(18,19,22,39)	19.0042
				D(18,19,22,40)	139.9828
				D(18,19,22,41)	-100.7824
				D(20,19,22,39)	-162.0699
				D(20,19,22,40)	-41.0913
				D(20,19,22,41)	78.1435
				D(19,20,21,16)	-0.5646
				D(19,20,21,38)	-179.059
				D(37,20,21,16)	179.3574
				D(37,20,21,38)	0.8629

TABLE-2
CALCULATED THERMODYNAMIC PARAMETERS AT B3LYP/6-311G(d,p) BASIS SET: ENTHALPY (H/a.u.), GIBBS FREE ENERGY (G/a.u.) AND ENTROPY [S/(cal/mol–K)] OF (**1**), (**2**), (**3**), (**4**) AND THEIR CHANGE FOR REACTION AT 25 °C

3-Acetyl coumarin (**1**)	*p*-Toluene sulfonyl hydrazide (**2**)	CHH (product) (**3**)	Water (byproduct) (**4**)	Δ values	Reaction
-649.709	-930.848	-1504.104	-76.444	ΔG	-0.009
-649.659	-930.798	-1504.025	-76.423	ΔH	0.009
105.486	104.830	165.799	45.116	ΔS	0.599

TABLE-3
TOPOLOGICAL PARAMETERS FOR VARIOUS INTRAMOLECULAR INTERACTIONS IN CHH CALCULATED AT B3LYP/6-311G(d,p) BASIS SET: ELECTRON DENSITY (ρ_{BCP}), LAPLACIAN OF ELECTRON DENSITY ($\nabla^2 \rho_{BCP}$), ELECTRON KINETIC ENERGY DENSITY (G_{BCP}), ELECTRON POTENTIAL ENERGY DENSITY (V_{BCP}), TOTAL ELECTRON ENERGY DENSITY (H_{BCP}), ESTIMATED HYDROGEN BOND OR OTHER WEAKER INTERACTION ENERGY (E_{int}) AT BOND CRITICAL POINT (BCP) OF CHH

Interaction modes	Rho $\rho_{(BCP)}$	$\nabla^2 \rho_{(BCP)}$	$G_{(BCP)}$	$V_{(BCP)}$	$H_{(BCP)}$	Bond ellipticity	E_{int} (Kcal/mol)
C8-O14···N12/C11-N12···O14	0.02676	0.11976	0.02586	-0.02178	0.00408	0.036512	-6.8335
C21-H38···H31/N13-H31···H38	0.00836	0.03422	0.00663	-0.00471	0.00192	0.562167	-1.4746
C10-H30···H32/C15-H32···H30	0.03840	0.09569	0.02791	-0.0319	-0.00398	0.184183	-10.0087

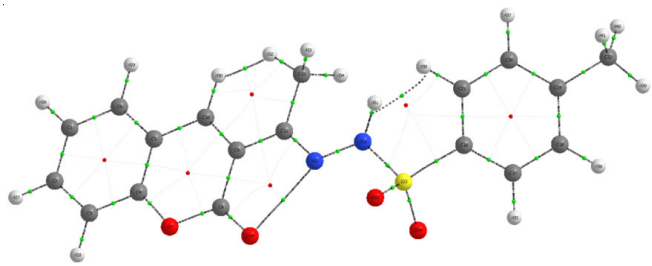

Fig. 2. Molecular graph of coumarin based hydrazide-hydrazone (CHH) derivative

C15/C15–H32···H30–C10) due to ($\nabla^2\rho_{BCP}$) > 0, H_{BCP} > 0 and $d_{H\cdots O}$ > (r_H + r_O). Both the interaction form a six membered ring (C15–H32···H30–C10–C9–C11) and (C21–H38···H31–N13–S23–C22). Another intramolecular van der Waal interaction between the interacting atoms (C8–O14···N12–O11) forms a five–membered ring (C8–O14···N12–O11–C9), producing S(5) ring motif. On the basis of interaction energy (E_{int}), the strength of the various interactions are in the following order: C21-H38···H31/N13-H31···H38 > C8-O14···N12/C11-N12···O14 > C10-H30···H32/C15-H32···H30.

^{1}H and ^{13}C NMR studies: For calculating ^{1}H and ^{13}C NMR chemical shifts of CHH GIAO technique has been applied at the B3LYP/6–31G(d,p) and B3LYP/6–311G(d,p) basis set. The molecular geometry of CHH has been optimized along with tetramethylsilane (TMS) [21]. The calculated and experimental ^{1}H & ^{13}C NMR chemical shifts (δ in ppm) for CHH are provided in Table-4. In order to compare the ^{1}H NMR chemical shifts, the correlation graphs between the experimental and calculated chemical shifts for CHH are shown in Fig. 3a and correlation graphs follow the linear equations, $y = 0.84651x - 0.49577$; $y = 0.90476x + 1.19579$, calculated at B3LYP/6–31G(d,p) and B3LYP/6–311G(d,p) basis set. The values of correlation coefficient ($R^2 = 0.83$ and 0.90) show that there is a good agreement between experimental and calculated results for CHH at B3LYP/6–311G(d,p) basis set. The experimental and calculated ^{13}C NMR chemical shifts (δ in ppm) are given in Table-5 and the correlation graph between the experimental and calculated ^{13}C

TABLE-4
EXPERIMENTAL AND THEORETICAL ^{1}H NMR CHEMICAL SHIFTS (δ, ppm) IN DMSO SOLVENT AT 25 °C AND B3LYP/6-31G(d,p)/B3LYP/6-311G(d,p) BASIS SET

Atom	δ calcd. 6-31G(d,p)	δ calcd. 6-311G(d,p)	δexp.	Assignment
26 H	6.1350	8.2487	7.89-7.75	Coumarin ring A and B
27 H	6.4233	8.5695		
28 H	6.2512	8.2092		
29 H	6.1324	8.4807		
30 H	6.1055	8.7022	7.89	C-H ring B
31 H	5.3983	8.2027	10.50	N-H azomethine framework
32 H	0.9432	2.9147	2.13	Me 2
33 H	0.5611	2.3846		
34 H	0.9072	2.8104		
35 H	6.8291	8.5750	7.47-7.16	Tosyl ring C
36 H	6.1541	8.2805		
37 H	6.3425	8.3187		
38 H	7.8928	9.2163		
39 H	0.9608	2.9160	2.23	Me 1
40 H	1.2857	3.1568		
41 H	1.5842	3.3407		

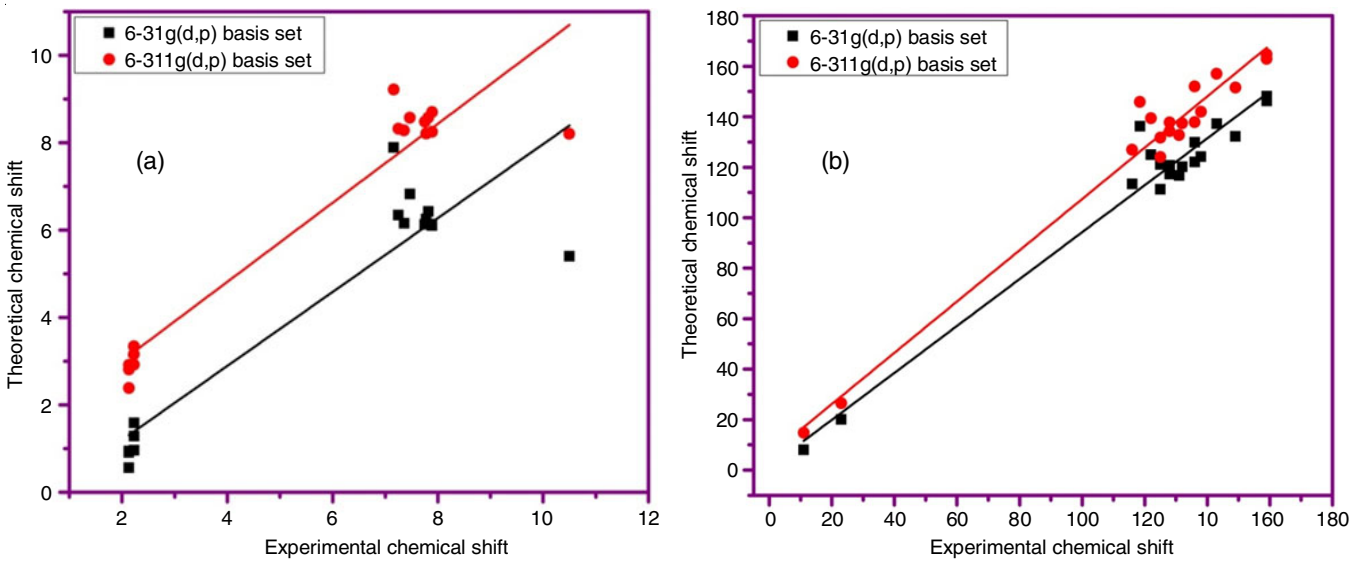

Fig. 3. Correlation graph of (a) ^{1}H NMR and (b) ^{13}C NMR for CHH

TABLE-5
EXPERIMENTAL AND THEORETICAL ^{13}C NMR CHEMICAL SHIFTS (δ, ppm) IN DMSO SOLVENT AT 25 °C AND B3LYP/6-31G(d,p)/ B3LYP/6-311G(d,p) BASIS SET

Atom	δ calcd. 6-31G(d,p)	δ calcd. 6-311G(d,p)	δexp.	Assignment
1 C	116.7138	132.7074	159-125	Coumarin ring A and B
2 C	124.1884	142.0063		
3 C	111.1967	123.9710		
4 C	148.1275	164.7047		
5 C	113.4178	126.9255		
6 C	120.7158	137.7425		
8 C	146.2973	162.9513		
9 C	121.1005	131.7095		
10 C	129.9160	152.0319		
11 C	132.2393	151.5656	149.200	(-C=) azomethine
15 C	8.0694	14.7748	11.000	Me2
16 C	136.2036	145.8501	143-118	Tosyl ring C
17 C	117.2607	134.2695		
18 C	120.1592	137.3821		
19 C	137.2450	157.0442		
20 C	122.0768	137.7942		
21 C	124.9819	139.4253		
22 C	20.0390	26.4435	23.000	Me 1

NMR chemical shifts are shown in Fig. 3b. The correlation graphs follow the linear equations: $y = 0.92952x + 1.33704$, $y = 1.01573x + 5.86212$, for ^{13}C NMR and correlation coefficients ($R^2 = 0.96$ and 0.97), again indicate good agreement between experimental and calculated results for CHH at B3LYP/6–311G(d,p) basis set.

Additional support about the structure of the synthesized CHH has been provided by the mass spectrum, which shows that the molecular ion's M+1 peak corresponds to its relative molecular mass. The estimated molecular mass of 356.40 for CHH was well-corroborated with the molecular mass 357.26 which was observed at M+1 in the experimental mass spectrum. The mass spectrum displays [M+1] peaks that line up with the chemical formula $C_{18}H_{16}N_2O_4S$.

FT-IR studies: The theoretical and experimental vibrational modes of CHH along with a PED assignment are given in Table-6 and the simulated spectrum is shown in Fig. 4. The CHH molecule consists of 41 atoms and 117 modes. The computed wavenumbers are scaled down using scaling factor 0.9608, 0.9668 for B3LYP/6–31G(d,p) and B3LYP/6–311G(d,p) basis set, respectively, in order to remove the anharmonicity present in the real system [25,26]. The measured wavenumbers are assigned by contrasting the estimated wavenumbers derived from the potential energy distribution (PED) study of the various vibrational modes.

C-H stretching: The CH_3 group is associated with the following vibrational modes: scissoring (δ_{sc}), rocking (δ_{ρ}), wagging (ω), twisting (t), asymmetric stretch (ν_{as}) and symmetric stretch (ν). Wagging and twisting deformations are indicative of depolarized out-of-plane vibration, scissoring and rocking are indicative of polarized in-plane vibration. The molecule has two methyl group with different environments. One of them is directly attached to the benzene ring; the second one is attached

TABLE-6
EXPERIMENTAL AND THEORETICAL (SELECTED) VIBRATIONAL WAVENUMBERS OF CHH USING B3LYP/6-31G(d,p) AND B3LYP/6-311G(d,p) BASIS SET AND THEIR ASSIGNMENTS [HARMONIC VIBRATIONAL WAVENUMBERS (cm^{-1}), IR_{int} (K $mmol^{-1}$)]

Mode No.	B3LYP/6-31G(d,p) wave. scaled	B3LYP/6-311G(d,p) wave. scaled	Exp. Wave	Assignments (%; > 5%)
117	3400	3409	3410	+(ν–$N_{13}H_{31}$)(100)
116	3207	3202		+(ν–$C_{21}H_{38}$)(97)
115	3199	3192		+(ν–$C_{17}H_{35}$)(96)
114	3198	3192		+(ν–C_3H_{28})(82)+(ν–C_2H_{27})(13)
113	3186	3181	3176	+(ν–C_1H_{26})(66)+(ν–C_2H_{27})(14)-(ν–C_3H_{28})(12)+(ν–C_6H_{29})(7)
112	3171	3166		+(ν–C_2H_{27})(62) -(ν–C_6H_{29})(14)-(ν–C_1H_{26})(11)-(ν–$C_{10}H_{30}$)(7)-(ν–C_3H_{28})(5)
111	3169	3164		+(ν–$C_{10}H_{30}$)(89)+(ν–C_2H_{27})(6)
110	3163	3157		+(ν–$C_{20}H_{37}$)(94)
109	3160	3156		+(ν–$C_{18}H_{36}$)(92)
107	3129	3120	3118	+(ν_{as}–$C_{15}H_{32}$)(89)-(ν–$C_{15}H_{33}$)(6)
106	3105	3095	3090	+(ν_{as}–$C_{22}H_{39}$)(64)-(ν_{as}–$C_{22}H_{40}$)(35)
105	3077	3068		+(ν_{as}–$C_{22}H_{40}$)(42)-(ν–$C_{22}H_{41}$)(42)+(ν_{as}–$C_{22}H_{39}$)(16)
104	3066	3056		+(ν–$C_{15}H_{34}$)(52)-(ν–$C_{15}H_{33}$)(48)
103	3017	3014	3012	+(ν–$C_{22}H_{41}$)(58)+(ν–$C_{22}H_{40}$)(23) +(ν–$C_{22}H_{39}$)(19)
102	3014	3010	3010	+(ν–$C_{15}H_{33}$)(46)+(ν–$C_{15}H_{34}$)(45) +(ν–$C_{15}H_{32}$)(9)
101	1825	1820	1747	+(ν–C_8O_{14})(83)-(ν–C_8C_9)(7)
100	1656	1649	1652	+(ν–$C_{11}N_{12}$)(30)-(ν–C_5C_6)(9)+(ν–C_5C_{10})(7)-(ν–C_9C_{10})(6)-(ν–C_2C_3)(6) + (ν–C_3C_4) (6)+(ν–C_1C_6) (5)
99	1648	1642	1640	+(ν–C_9C_{10})(28)-(ν–C_4C_5)(12)+(ν–C_1C_6)(10)-(δ_{ip}–$C_9H_{30}C_{10}C_5$)(8)-(ν–C_1C_2)(7)+(ν–C_3C_4)(6)+(δ'_{as}–ringA)(5)
97	1640	1631	1630	+(ν–$C_{20}C_{21}$)(21)+(ν–$C_{17}C_{18}$)(20) +(δ_{as}–ringC)(10)-(ν–$C_{19}C_{20}$)(8)-(ν–$C_{18}C_{19}$)(7)-(δ_{ip}–$C_{21}C_{19}C_{20}H_{37}$)(7) +(δ_{ip}–$C_{18}C_{17}C_{19}H_{36}$)(6)
96	1614	1608		+(ν–$C_{16}C_{17}$)(20)-(ν–$C_{16}C_{21}$)(18)-(ν-$C_{18}C_{19}$)(18) +(ν–$C_{19}C_{20}$)(15)-(δ'_{as}–ringC)(9)
95	1598	1591	1595	+(ν–C_9C_{10})(20)+(ν–C_1C_2)(13)+(ν–C_4C_5)(12)-(ν–C_2C_3)(11)-(δ_{ip}–$C_3H_{27}C_1C_2$)(9)-(ν–C_5C_{10})(6)
94	1525	1520	1521	+(δ_{ip}–$C_{21}C_{16}C_{20}H_{38}$)(21)-(δ_{ip}–$C_{18}C_{17}C_{16}H_{35}$)(15)+(δ_{ip}–$C_{21}C_{19}C_{20}H_{37}$)(12)-(δ_{ip}–$C_{18}C_{17}C_{19}H_{36}$)(12)-(ν–$C_{16}C_{21}$)(10)-(ν–$C_{16}C_{17}$)(9)+(ν–$C_{19}C_{20}$)(8)+(ν–$C_{18}C_{19}$)(6)
93	1517	1510	1515	+(δ_{ip}–$C_5H_{29}C_1C_6$)(17)-(δ_{ip}–$C_3H_{28}C_4C_2$)(16)-(ν–C_4C_5)(13)+(ν–C_5C_{10})(10)+(δ_{ip}–$C_6H_{26}C_1C_2$)(9)+(ν–C_1C_2)(9)-(ν–C_5C_6)(7)+(ν–C_2C_3)(5)
92	1509	1506	1502	+(δ'_{as}–$H_{32}H_{33}H_{34}C_{15}C_{11}$)(69)-($\delta'_{as}$–$H_{32}H_{33}H_{34}C_{15}C_{11}$)(15)
91	1493	1489	1490	+(δ'_{as}–$H_{39}H_{40}H_{41}C_{19}C_{22}$)(52) +($\delta_{as}$–$H_{39}H_{40}H_{41}C_{19}C_{22}$)(29)-($\delta\rho$-$H_{39}H_{40}H_{41}C_{19}C_{22}$)(8)
90	1489	1484		+(δ_{as}–$H_{39}H_{40}H_{41}C_{19}C_{22}$)(60)-($\delta'_{as}$–$H_{39}H_{40}H_{41}C_{19}C_{22}$)(28)-($\delta'\rho$-$H_{39}H_{40}H_{41}C_{19}C_{22}$)(7)
89	1486	1482	1486	+(δ_{as}–$H_{32}H_{33}H_{34}C_{15}C_{11}$)(36) +($\delta_{ip}$–$C_3H_{27}C_1C_2$)(10)+($\delta_{ip}$–$C_6H_{26}C_1C_2$)(10)+(ν–$C_3C_4$)(5)-(ν–$C_5C_6$)(5)+($\delta_{as}$–$H_{32}H_{33}H_{34}C_{15}C_{11}$)(38)-($\delta_{ip}$–$C_3H_{27}C_1C_2$)(10)-($\delta_{ip}$–$C_6H_{26}C_1C_2$)(9)+($\delta'_{as}$–$H_{32}H_{33}H_{34}C_{15}$C11)(8)-(ν–$C_3C_4$)(5)
87	1431	1426	1422	+(ν–$C_{17}C_{18}$)(21)-(ν–$C_{20}C_{21}$)(19) +(δ_{ip}–$C_{21}C_{19}C_{20}H_{37}$)(11)+(δ_{ip}–$C_{18}C_{17}C_{19}H_{36}$)(10)-(δ_{ip}–$C_{18}C_{17}C_{16}H_{35}$)(9)-(δ_{ip}–$C_{21}C_{16}C_{20}H_{38}$)(9)+(δ'_{as}–$H_{39}H_{40}H_{41}C_{19}C_{22}$)(8)
86	1415	1409	1410	+(δ_s–$H_{39}H_{40}H_{41}C_{19}C_{22}$)(88)+(ν–$C_{19}C_{22}$)(8)
85	1413	1409		+(δ_s–$H_{32}H_{33}H_{34}C_{15}C_{11}$)(64)-($\delta'_{as}$–$H_{32}H_{33}H_{34}C_{15}C_{11}$)(9)-($\delta_{ip}$–$N_{12}N_{13}S_{23}H_{31}$)(9)+(ν–$C_{11}C_{15}$)(6)
84	1388	1392	1390	+(δ_{ip}–$N_{12}N_{13}S_{23}H_{31}$)(50)-(δ_{ip}–$C_9H_{30}C_{10}C_5$)(9)+(δ_s–$H_{32}H_{33}H_{34}C_{15}C_{11}$)(6)
82	1374	1362	1355	+(ν–C_1C_6)(18)+(ν–C_2C_3)(17)+(ν–C_4C_5)(14)-(ν–C_1C_2)(10)-(ν–C_3C_4)(10)-(ν–C_5C_6)(8)
78	1317	1310	1290	+(ν_{as}–$S_{23}O_{25}$)(39)-(ν_{as}–$S_{23}O_{24}$)(30)
76	1275	1273	1270	+(δ_{tri}–ringA)(19)+(ν–C_5C_{10})(18)-(ν–C_4O_7)(17)-(δ_{ip}–$C_9H_{30}C_{10}C_5$)(11) +(δ_{ip}–$C_3H_{28}C_4C_2$)(8)-(ν–C_3C_4)(7)-(δ_{tri}–ringB)(5)
75	1243	1239		+(δ_{ip}–$C_9H_{30}C_{10}C_5$)(25)+(ν–C_5C_6)(22)+(δ_{ip}–$C_5H_{29}C_1C_6$)(16)-(ν–C_4O_7)(7)-(ν–C_9C_{11})(5)
71	1138	1138		+(δ_{ip}–$C_3H_{27}C_1C_2$)(16)+(ν–C_1C_6)(12)-(δ_{ip}–$C_3H_{28}C_4C_2$)(12)-(ν–C_2C_3)(11)+(δ_{ip}–$C_6H_{26}C_1C_2$)(8)-(δ_{ip}–$C_5H_{29}C_1C_6$)(7)+(δ_{tri}–ringA)(6)
69	1137	1132	1137	+(ν–$S_{23}O_{24}$)(24)+(ν–$S_{23}O_{25}$)(22)-(ν–$C_{16}S_{23}$)(13)+(ν–$C_{16}C_{21}$)(5)+(ν–$C_{16}C_{17}$)(5)-(δ_{ip}–$C_{18}C_{17}C_{16}H_{35}$)(5)

68	1130	1125	1130	+(ν–$N_{12}N_{13}$)(54)-(δ–$N_{12}C_{11}C_9C_{15}$)(10)-(ν–$C_{11}C_{15}$)(6)
66	1079	1075	1080	+(ν–$S_{23}O_{24}$)(21)-(ν–$C_{16}C_{21}$)(17)+(ν–$S_{23}O_{25}$)(16)-(ν–$C_{16}C_{17}$)(15)+(ν–$C_{16}S_{23}$)(7) +(δ_{ip}–$C_{18}C_{17}C_{16}H_{35}$)(5)
65	1056	1058	1060	+(δ'ρ-$H_{39}H_{40}H_{41}C_{19}C_{22}$)(55)-(ω–$C_{18}C_{20}C_{19}C_{22}$)(10)+(δρ-$H_{39}H_{40}H_{41}C_{19}C_{22}$)(8) -($\tau_{puckering}$–ringC)(7)+($\delta_{as}$–$H_{39}H_{40}H_{41}C_{19}C_{22}$)(5)+(ω–$C_{18}C_{17}C_{19}H_{36}$)(5) (ω–$C_{21}C_{19}C_{20}H_{37}$)(5)
64	1046	1044		+(ν–C_1C_2)(42)+(δ_{ip}–$C_3H_{28}C_4C_2$)(15)+(ν–C_2C_3)(12)+(ν–C_1C_6)(10)-(δ_{ip}–$C_5H_{29}C_1C_6$)(9)
63	1039	1039	1041	+(δ'ρ-$H_{32}H_{33}H_{34}C_{15}C_{11}$)(63)-(ω–$N_{12}C_{11}C_9C_{15}$)(12)-(δρ-$H_{32}H_{33}H_{34}C_{15}C_{11}$)(8)
62	1024	1029	1027	+(δ_{tri}–ringC)(61)-(ν–$C_{18}C_{19}$)(10)-(ν–$C_{19}C_{20}$)(6)
60	1007	1000	1003	+(δρ-$H_{39}H_{40}H_{41}C_{19}C_{22}$)(62)+(ν–$C_{19}C_{20}$)(10)-(δ'ρ-$H_{39}H_{40}H_{41}C_{19}C_{22}$)(8)-(ν–$C_{18}C_{19}$)(5)
56	952	958		+(ω–$C_5H_{29}C_1C_6$)(29)+(ω–$C_9H_{30}C_{10}C_5$)(27)+(ω–$C_3H_{28}C_4C_2$)(13)-(ω–$C_3H_{27}C_1C_2$)(9)-(ω–$C_6H_{26}C_1C_2$)(8)-(τ'$_{as}$–ringA)(5)
54	931	932		+(ν–O_7C_8)(20)-(δ_{tri}–ringA)(52)-(ν–$C_{11}C_{15}$)(16)+(ω–$C_9H_{30}C_{10}C_5$)(18)+(ω–$C_6H_{26}C_1C_2$)(11)-(ω–$C_3H_{28}C_4C_2$)(10)-(ω–$C_5H_{29}C_1C_6$)(6)
53	915	912		+(δ_{tri}–ringA)(32)+(δ_{tri}–ringB)(21)-(ν–$C_{11}C_{15}$)(12)+(ν–O_7C_8)(8)-(δ_{ip}–$O_{14}O_7C_9C_8$)(7)
52	874	874	860	+(ν–$N_{13}S_{23}$)(15)-(δ–$N_{12}N_{13}S_{23}H_{31}$)(14)+(δ_{as}–$C_{11}N_{12}N_{13}$)(11)-(δρ-$H_{32}H_{33}H_{34}C_{15}C_{11}$)(9)+(ω–$N_{12}N_{13}S_{23}H_{31}$)(6)
49	835	834	830	+(ν–$N_{13}S_{23}$)(14)+(ν–C_4C_5)(8)+(ν–C_5C_6)(8)+(ν–C_5C_{10})(7)-(ν–C_9C_{11})(6)-(ν–$N_{12}N_{13}$)(6)+(δ_{tri}–ringB)(5)
48	825	823		+(ω–$C_{18}C_{17}C_{19}H_{36}$)(29)+(ω–$C_{18}C_{17}C_{16}H_{35}$)(21)+(ω–$C_{21}C_{19}C_{20}H_{37}$)(17)+(ω–$C_{21}C_{16}C_{20}H_{38}$)(12)+(τ_{as}–ringC)(7)-(ω–$CC_{21}C_{16}C_{17}S_{23}$)(5)
45	759	764	750	+(ω–$O_{14}O_7C_9C_8$)(31)-($\tau_{puckering}$–ringB)(25)-(ω–$C_9C_{10}C_8C_{11}$)(17)-(ω–$C_6H_{26}C_1C_2$)(5)
42	710	713	718	+($\tau_{puckering}$–ringC)(69)-(ω–$CC_{21}C_{16}C_{17}S_{23}$)(10)+(ω–$C_{18}C_{20}C_{19}C_{22}$)(9)
41	676	676	670	+(δ_{tri}–ringB)(10)+(ν–$C_{11}C_{15}$)(9) +(δ'$_{as}$–ringA)(9)-(ν–$N_{13}S_{23}$)(9)+(δ_{ip}– $N_{12}C_{11}C_9C_{15}$)(8)-ω-($C_{16}S_{23}O_{24}O_{25}N_{13}$)(8)+($\delta_{as}$–$C_{11}N_{12}N_{13}$)(7)+(ν–$C_9C_{11}$)(5)
40	642	645	643	+(δ'$_{as}$–ringC)(68)
39	637	640	641	+(δ_{as}–ringA)(20)+(δ_{ip}–$O_{14}O_7C_9C_8$)(13)+(δ'$_{as}$–ringC)(11) +(δ_{ip}–$9C_{10}C_8C_{11}$)(7)-(ν–$C_{16}S_{23}$)(6)
38	634	635		(ν–$C_{16}S_{23}$)(14)+(δ_{as}–ringA)(13)+(ν–$N_{13}S_{23}$)(8)(δ_{as}–ringC)(8)-(ν–$C_{19}C_{22}$) (7)+δ_{ip}-Methylene(5) -(δ_{tri}–ringC)(5)
36	588	588		+(δ'$_{as}$–ringA)(28)-(ω–$N_{12}N_{13}S_{23}H_{31}$)(12)-(τ–$C_{11}N_{12}N_{13}H_{31}$)(11)+(ν–$N_{13}S_{23}$)(6)-(δ'$_{as}$–ringB)(5)
35	566	568		+(ω–$N_{12}C_{11}C_9C_{15}$)(11)-(δ_{as}–ringB)(9)-(δ'$_{as}$–ringB)(7)+(τ_{as}–ringC)(5)-ω-($C_{16}S_{23}O_{24}O_{25}N_{13}$)(5)-(ω–$CC_{21}C_{16}C_{17}S_{23}$)(5)-$\delta_{ip}$-Methylene(5)
34	558	560	550	+(τ_{as}–ringA)(22)+($\tau_{puckering}$–ringA) (17)-($\tau_{puckering}$–ringB)(10)-(ω–$N_{12}N_{13}S_{23}H_{31}$)(5)+(ω–$C_6H_{26}C_1C_2$) (5)
33	548	550		+(τ_{as}–ringA)(11)+(ω–$N_{12}C_{11}C_9C_{15}$)(9)+(δ_{as}–ringB)(6)-δ_{ip}-Methylene(5) +($\tau_{puckering}$–ringA)(5)
32	520	524	522	+(ω-$C_{16}S_{23}O_{24}O_{25}N_{13}$)(12)-($\tau_{as}$–ringC)(10)+(ω–$N_{12}C_{11}C_9C_{15}$)(8)+(ω–$CC_{21}C_{16}C_{17}S_{23}$)(7)-(τ–$C_9C_{11}N_{12}N_{13}$)(6)+($\delta_{ip}$–$N_{12}C_{11}C_9C_{15}$)(5)+(ω–$C_{18}C_{20}C_{19}C_{22}$)(5)
31	507	505		+(ω–$N_{12}N_{13}S_{23}H_{31}$)(17)+δ_{ip}-Methylene(12)+(τ–$C_{11}N_{12}N_{13}H_{31}$)(11)+(ω–$N_{12}C_{11}C_9C_{15}$)(10)-(ω-$C_{16}S_{23}O_{24}O_{25}N_{13}$)(7)-($\delta_{as}$–ringC)(6)-(ω–$C_9C_{10}C_8C_{11}$)(6)-(τ–$C_9C_{11}N_{12}N_{13}$)(5)-(τ–$C_{10}C_9C_{11}C_{15}$)(5)
30	502	501		+(τ_{as}–ringC)(22)+δρ-($C_{16}S_{23}O_{24}O_{25}N_{13}$)(19)-(ω–$CC_{21}C_{16}C_{17}S_{23}$)(13)-(ω–$C_{18}C_{20}C_{19}C_{22}$)(11)+(δ–$N_{12}N_{13}S_{23}H_{31}$)(6)

ν– stretching, ρ–rocking, ω–wagging, δ–deformation, δ_{as}–asymmetric deformation, τ– twisting, δ_{tri}– trigonal deformation, ip– in-plane, oop– out-of-plane

to azomethine carbon atom named as Me1 and Me2, respectively. Symmetric band stretching for Me1 methyl group ($\nu_{C\text{-}H}$) observed at 3010 cm^{-1} and the calculated wavenumber for this vibration found at 3014 cm^{-1} and 3010 cm^{-1} in at B3LYP/6-31G-(d,p) and at B3LYP/6-311G(d,p), respectively, with 100% PED contribution. A symmetric band stretching for Me2 methyl group found ($\nu_{C\text{-}H}$) at 3012 cm^{-1} and the calculated wavenumber for this vibration found at 3017 cm^{-1} and 3014 cm^{-1} in B3LYP/6-31G(d,p) and B3LYP/6-311G(d,p), respectively with 100% PED contribution. The asymmetric stretching vibration ($\nu_{C\text{-}H}$) of methyl group observed in between 3090-3060 cm^{-1} for Me1 and 3118 cm^{-1} for Me2. The asymmetric deformation (δ_{as}) for Me1 and Me2 observed at 1490 cm^{-1} and 1502 cm^{-1} which correlate well with the calculated wavenumber for this vibration found at 1493 cm^{-1} and 1509 cm^{-1} in B3LYP/6-31G(d,p) and 1488 cm^{-1} and 1506 cm^{-1} in B3LYP/6-311G(d,p), respectively,

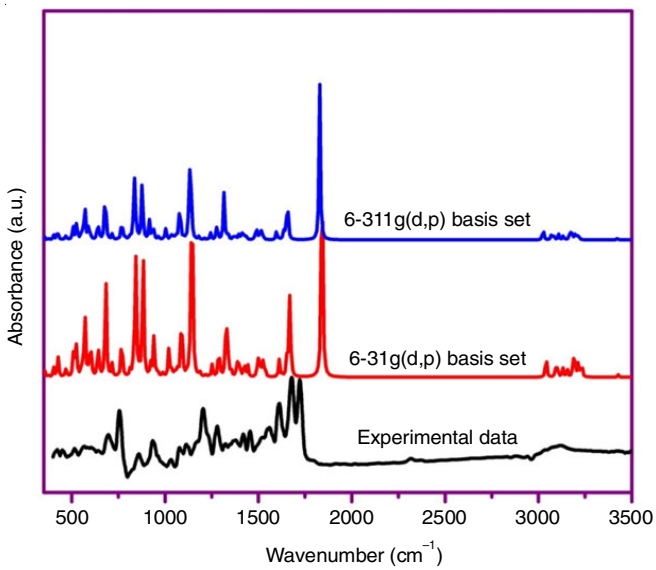

Fig. 4. Simulated (computational and experimental) FT-IR spectrum for CHH

with 89% and 84% PED contribution. The symmetric stretching vibration of coumarin ring A, B and phenyl ring C is observed in the range of 3200-3150 cm^{-1}.

C-C and C=C stretching: The C-C asymmetric stretching vibration of coumarin ring (A, B) observed at 1640 cm^{-1}. The tosyl ring that is abbreviated as ring C shows C=C asymmetric stretching vibrations (Ar- $\nu_{C-C,\ C=C}$) at 1630 cm^{-1}, asymmetric stretching calculated at 1648, 1640 cm^{-1} for B3LYP/6-31G(d,p) and 1642, 1631 cm^{-1} for B3LYP/6-311G(d,p) with 68% and 66% contribution in PED, respectively. The rocking vibration ($\nu_{C=C}$) of ring A, B and tosyl ring C observed at 1515 cm^{-1} and 1521 cm^{-1}, which well corresponds to the calculated wavenumber at 1517, 1525 cm^{-1} (B3LYP/6-31G(d,p)) and 1510, 1520 cm^{-1} (B3LYP/6-311G(d,p)) basis set. Puckering for coumarin ring A, B and tosyl ring C observed at 550 cm^{-1} and 718 cm^{-1}, which is well correlated with calculated wavenumber at 558 cm^{-1}, 710 cm^{-1} for B3LYP/6-31G(d,p) and 560 cm^{-1}, 713 cm^{-1} for B3LYP/6-311G(d,p) basis set, respectively.

C=N stretching: The observed C=N stretching vibration ($\nu_{C=N}$) at 1652 cm^{-1} corresponds to the calculated wavenumber at 1656 cm^{-1}, 1649 cm^{-1} for B3LYP/6-31G(d,p) and B3LYP/6-311G(d,p) basis set. The observed experimental wavenumber is well corroborated with calculated wavenumber obtained by B3LYP/6-311G(d,p) basis set. In FT-IR spectrum, the presence of C=N band confirms the presence of hydrazone linkage in the synthesized compound CHH.

N–N and N-H stretching: The N-N stretching vibration is observed at 1130 cm^{-1}, whereas it is calculated at 1030 cm^{-1} for B3LYP/6-31G(d,p) 1025 cm^{-1} in B3LYP/6-311G(d,p) in theoretical spectrum. The N-H stretching of azomethine group found at 3410 cm^{-1} with 100% PED contribution show correspondence to the calculated wavenumber at 3400 cm^{-1} for B3LYP/6-31G(d,p) and 3409 cm^{-1} for B3LYP/6-311G(d,p) basis set.

S-O vibration: The observed bands at around 1290 cm^{-1} and 1137 cm^{-1} in CHH are assigned to the (SO_2) asym. and (SO_2) sym. The modes show correspondence to the calculated wavenumber at 1317, 1137 cm^{-1} for B3LYP/6-31G(d,p) and 1310, 1132 cm^{-1} in B3LYP/6-311G(d,p) basis set. Some wavenumber assigned to SO_2 scissoring and SO_2 wagging vibrations in all the synthesized compounds and have partly overlapped in this region; the calculations show that wagging (SO_2) vibration contains a considerable contribution with π-ring and NH bending vibrations.

C=O stretching: The C=O stretching vibration is observed at 1747 cm^{-1}, whereas it was calculated at 1825 cm^{-1} for B3LYP/6-31G(d,p) 1820 cm^{-1} in B3LYP/6-311G(d,p) basis set in the theoretical spectrum with 83% PED contribution.

UV-visible studies: Using TD-DFT calculation has been used to study the nature of excitations in the UV-visible spectrum of CHH molecule at B3LYP/6-31G(d,p) and B3LYP/6-311G (d,p) basis [27,28] and are listed in Table-7. The simulated UV-visible spectrum is given in Fig. 5. The band gap can be estimated by using the equation: $E_{L-H} = E_{LUMO} - E_{HOMO}$. The energies of HOMO and LUMO and their neighboring orbitals are negative, which indicates that CHH molecule is stable [29]. The HOMO – LUMO energy gap 3.91865, 4.04991 eV of CHH molecule calculated at B3LYP/6-31G(d,p) and B3LYP/6-311G (d,p) basis set, respectively, reflects the chemical stability of

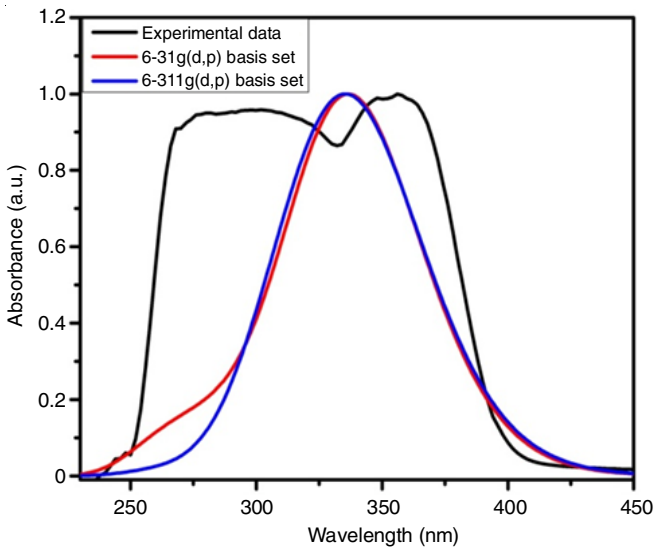

Fig. 5. Simulated computational and experimental UV-vis spectrum of synthesized CHH

TABLE-7
EXPERIMENTAL AND CALCULATED (EXCITATION ENERGIES (eV), OSCILLATOR STRENGTHS (f), ASSIGNMENTS) WAVELENGTH (λ) OF CHH AT B3LYP/6–31G(d,p) AND B3LYP/6–311G(d,p) BASIS SET

Orbitals	Basis set 6-31g(d,p)			Basis set 6-311g(d,p)			Exp. λ	Assig.
	Energy	λ (nm)	f	Energy	λ (nm)	f		
H→L	3.6657	338.23	0.5693	3.6702	337.81	0.7411	350	π→π*
H-5→L	4.6916	264.27	0.0520	4.6928	264.20	0.0107	260	π→π*

the molecule. The molecular orbital plots calculated at B3LYP/6-31G(d,p) and B3LYP/6-311G(d,p) basis set are shown in Fig. 6. It was observed that, the electron clouds of HOMO are mainly located on the tosyl ring and LUMO orbitals are mainly concentrated on carbonyl group of coumarin moiety when calculated at B3LYP/6-31G(d,p) basis set whereas in case of B3LYP/6-311G(d,p), the LUMO orbitals are located on the junction of coumarin moiety. The TD-DFT calculations predict one intense and one broad electronic transitions at λ_{max} = 338.23 nm, f = 0.5693, λ = 264.27 nm, f = 0.0520 at B3LYP/6-31G (d,p) basis set and at λ_{max} = 337.81 nm, f = 0.7411, λ = 264.20 nm, f = 0.0107 at B3LYP/6-311G(d,p) basis set. In the experimental spectrum, the observed λ_{max} at 350 nm is in good agreement with the calculated λ_{max} at 338.23 and 337.81 nm calculated at B3LYP/6–31G(d,p) and B3LYP/6–311G(d,p) basis set, respectively. The TD–DFT calculations show that the experimental band at 350 nm originates mainly due to H→L transition and 260 nm due to H-5→L transition for CHH molecule. On the basis of the molecular orbital coefficients analyses and molecular orbital plots the nature of these electronic transitions are assigned to $\pi \rightarrow \pi^*$. In the experimental UV-visible spectrum, the observed λ_{max} at 350 nm is slightly red shifted compared with the calculated λ_{max} at 338.23 and 337.81 on both basis set.

Natural bond orbital (NBO): One of the useful features of NBOs is that they provide a precise method for analyzing intramolecular bonding and bond-to-bond contact, as well as an efficient basis for studying conjugative interaction or charge transfer in a range of molecular systems [30]. The higher second order stabilization energy ($E^{(2)}$) value indicates a stronger connection between electron donors and acceptors. The delocalization of electron density between formally vacant (antibond or Rydgberg) non-Lewis NBO orbitals and occupied Lewis-type (bond or lone pair) NBO orbitals represents a stabilizing donor-acceptor interaction. To get a quantitative characterization of the intramolecular interactions listed in Table-8, a second-order perturbation theory is applied to determine the energy lowering associated with those interactions. For each donor NBO(i) and acceptor NBO(j), the second order energy lowering equation, which is described below, estimates the strength of various interactions or stabilizing energy ($E^{(2)}$) related to electron delocalization between donor and acceptor [31,32].

$$E^{(2)} = -q_i \frac{(F_{ij})^2}{\varepsilon_j - \varepsilon_i}$$

where q_i is the population of donor orbital or donor orbital occupancy; ε_i, ε_j are the orbital energies of donor and acceptor NBO orbitals, respectively; F_{ij} is the off-diagonal Fock or Kohn-Sham matrix element between i and j NBO orbitals. Diverse forms of "orbital–orbital" and "loan pair–orbital" overlap give rise to distinct intramolecular interactions. The $\pi \rightarrow \pi^*$ interactions involve the π-conjugation and resonance resulting from π-electron delocalization in rings, while the $\sigma \rightarrow \sigma^*$ orbital overlap accounts for the primary hyperconjugative interactions and the secondary hyperconjugative interactions [33] are caused by the different types of orbital overlaps, including $\sigma \rightarrow \sigma^*$, $\pi \rightarrow \sigma^*$ and $n \rightarrow \sigma^*$. The interactions π(C4-C5)→π^*(C9-C10),

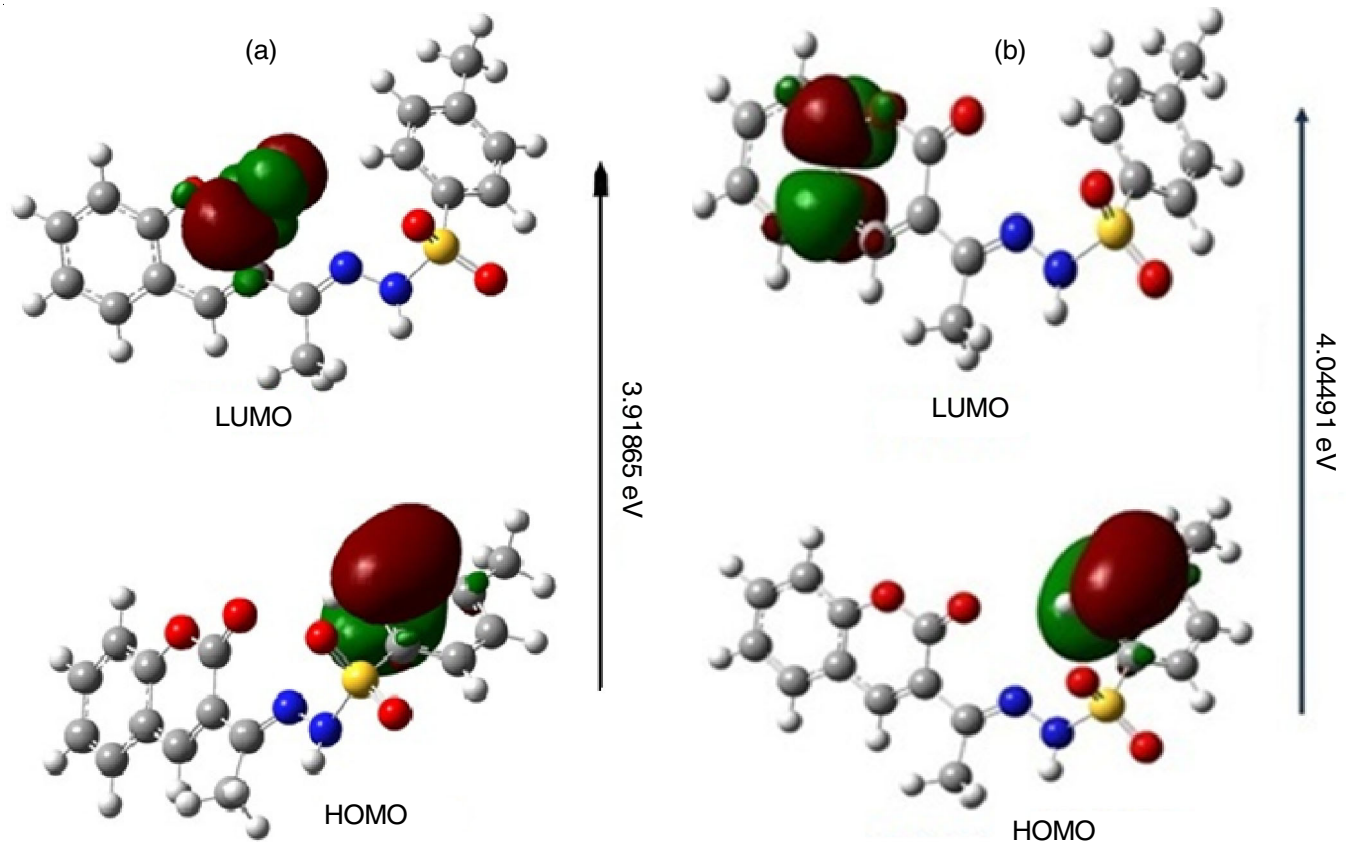

Fig. 6. Selected molecular orbital plot involved in electronic excitations for CHH calculated at (a) B3LYP/6-31G(d,P) and (b) B3LYP/6-311G(d,P) basis set

TABLE-8
SECOND-ORDER PERTURBATION THEORY ANALYSIS OF THE FOCK MATRIX IN NBO BASIS FOR THE CHH: SELECTED DONOR (LEWIS) AND ACCEPTOR (NON-LEWIS) ORBITALS, PERCENTAGE ELECTRON DENSITY OVER BONDED ATOMS (ED_X, %), NBO HYBRID ORBITALS OF BONDED ATOMS AND STABILIZATION ENERGY OF VARIOUS INTERMOLECULAR INTERACTIONS ($E^{(2)}$) for [B3LYP/6-31G(d,p)] AND [B3LYP/6-311G(d,p)] BASIS SET

Donor (i)			Acceptor (j) [6-31G(d,p)]			$E^{(2)}$ (kcal/mol)	Acceptor (j) [6-311G(d,p)]			$E^{(2)}$ (kcal/mol)
(Occupancy) (i)	ED_A % ED_B %	NBO hybrid orbitals	(Occupancy) (i)	ED_A % ED_B %	NBO hybrid orbitals		(Occupancy) (i)	ED_A % ED_B %	NBO hybrid orbitals	
$\pi(C_1–C_6)$ (1.70194)	51.20 48.80	0.7155 $(sp^{1.00})_C$ 0.6986 $(sp^{1.00})_C$	$\pi^*(C_2–C_3)$ (0.30748)	52.44 47.56	0.7242 $(sp^{1.00})_C$ -0.6896 $(sp^{1.00})_C$	21.32	$\pi^*(C_2–C_3)$ (0.31187)	51.83 48.17	0.7199 $(sp^{1.00})_C$ -0.6940 $(sp^{1.00})_C$	20.86
			$\pi^*(C_4–C_5)$ (0.44281)	53.76 46.24	0.7332 $(sp^{1.00})_C$ -0.6800 $(sp^{1.00})_C$	17.73	$\pi^*(C_4–C_5)$ (0.43579)	54.20 45.80	0.7362 $(sp^{1.00})_C$ -0. 6768 $(sp^{1.00})_C$	17.46
$\pi(C_2–C_3)$ (1.68353)	48.17 51.83	0.6940$(sp^{1.00})_C$ 0.7199$(sp^{1.00})_C$	$\pi^*(C_1–C_6)$ (0.28400)	48.62 51.38	0.6973 $(sp^{1.00})_C$ -0.7168 $(sp^{1.00})_C$	16.82	$\pi^*(C_1–C_6)$ (0.29912)	48.80 51.20	0.6986 $(sp^{1.00})_C$ -0.7155 $(sp^{1.00})_C$	17.70
			$\pi^*(C_4–C_5)$ (0.44281)	53.76 46.24	0.7332 $(sp^{1.00})_C$ -0.6800 $(sp^{1.00})_C$	23.22	$\pi^*(C_4–C_5)$ (0.43579)	54.20 45.80	0.7362 $(sp^{1.00})_C$ -0. 6768 $(sp^{1.00})_C$	22.79
$\pi(C_4–C_5)$ (1.58960)	46.24 53.76	0.6800 $(sp^{1.00})_C$ 0.7332 $(sp^{1.00})_C$	$\pi^*(C_1–C_6)$ (0.28400)	48.62 51.38	0.6973 $(sp^{1.00})_C$ -0.7168 $(sp^{1.00})_C$	18.31	$\pi^*(C_1–C_6)$ (0.29912)	48.80 51.20	0.6986 $(sp^{1.00})_C$ -0.7155 $(sp^{1.00})_C$	19.27
			$\pi^*(C_2–C_3)$ (0.30748)	52.44 47.56	0.7242 $(sp^{1.00})_C$ -0.6896 $(sp^{1.00})_C$	15.88	$\pi^*(C_2–C_3)$ (0.31187)	51.83 48.17	0.7199 $(sp^{1.00})_C$ -0.6940 $(sp^{1.00})_C$	16.27
			$\pi^*(C_9–C_{10})$ (0.20000)	44.58 55.42	0.6677 $(sp^{99.99})_C$ -0.7445 $(sp^{1.00})_C$	17.52	$\pi^*(C_9–C_{10})$ (0.20250)	46.46 53.54	0.6816 $(sp^{1.00})_C$ -0.7317 $(sp^{1.00})_C$	17.06
$\pi(C_9–C_{10})$ (1.77447)	55.42 44.58	0.7445 $(sp^{99.00})_C$ 0.6677 $(sp^{1.00})_C$	$\pi^*(C_4–C_5)$ (0.44281)	53.76 46.24	0.7332 $(sp^{1.00})_C$ -0.6800 $(sp^{1.00})_C$	11.24	$\pi^*(C_4–C_5)$ (0.43579)	54.20 45.80	0.7362 $(sp^{1.00})_C$ -0. 6768 $(sp^{1.00})_C$	11.73
			$\pi^*(C_8–O_{14})$ (0.28839)	69.54 30.46	0.8339 $(sp^{99.99})_C$ -0.5519 $(sp^{99.99})_O$	24.13	$\pi^*(C_8–O_{14})$ (0.25335)	68.02 31.98	0.8247 $(sp^{1.00})_C$ -0.5655 $(sp^{99.99})_O$	20.53
			$\pi^*(C_{11}–N_{12})$ (0.21312)	56.94 43.06	0.7546 $(sp^{99.99})_C$ -0.6562 $(sp^{99.99})_N$	16.87	$\pi^*(C_{11}–N_{12})$ (0.21760)	55.54 44.46	0.7453 $(sp^{99.99})_C$ -0.6668 $(sp^{99.99})_N$	15.54
$\pi(C_{16}–C_{17})$ (1.70245)	57.40 42.60	0.7576 $(sp^{1.00})_C$ 0.6527 $(sp^{1.00})_C$	$\pi^*(C_{18}–C_{19})$ (0.31959)	47.69 52.31	0.6906 $(sp^{1.00})_C$ -0.7233 $(sp^{1.00})_C$	14.82	$\pi^*(C_{18}–C_{19})$ (0.33299)	47.74 52.26	0.6909 $(sp^{1.00})_C$ -0.7229 $(sp^{1.00})_C$	15.16
			$\pi^*(C_{20}–C_{21})$ (0.28760)	48.00 52.00	0.6928 $(sp^{1.00})_C$ -0.7211 $(sp^{1.00})_C$	20.55	$\pi^*(C_{20}–C_{21})$ (0.28421)	47.16 52.84	0.6867 $(sp^{1.00})_C$ -0.7269 $(sp^{1.00})_C$	21.23
$\pi(C_{18}–C_{19})$ (1.62306)	52.31 47.69	0.7233 $(sp^{1.00})_C$ 0.6906 $(sp^{1.00})_C$	$\pi^*(C_{16}–C_{17})$ (0.40057)	42.60 57.40	0.6527 $(sp^{1.00})_C$ -0.7576 $(sp^{1.00})_C$	26.98	$\pi^*(C_{16}–C_{17})$ (0.39261)	42.84 57.16	0.6545 $(sp^{1.00})_C$ -0.7561 $(sp^{1.00})_C$	26.32
			$\pi^*(C_{20}–C_{21})$ (0.28760)	48.00 52.00	0.6928 $(sp^{1.00})_C$ -0.7211 $(sp^{1.00})_C$	17.53	$\pi^*(C_{20}–C_{21})$ (0.28421)	47.16 52.84	0.6867 $(sp^{1.00})_C$ -0.7269 $(sp^{1.00})_C$	17.08
$\pi(C_{20}–C_{21})$ (1.65479)	52.00 48.00	0.7211 $(sp^{1.00})_C$ 0.6928 $(sp^{1.00})_C$	$\pi^*(C_{16}–C_{17})$ (0.40057)	42.60 57.40	0.6527 $(sp^{1.00})_C$ -0.7576 $(sp^{1.00})_C$	18.34	$\pi^*(C_{16}–C_{17})$ (0.39261)	42.84 57.16	0.6545 $(sp^{1.00})_C$ -0.7561 $(sp^{1.00})_C$	18.93
			$\pi^*(C_{18}–C_{19})$ (0.31959)	47.69 52.31	0.6906 $(sp^{1.00})_C$ -0.7233 $(sp^{1.00})_C$	21.93	$\pi^*(C_{18}–C_{19})$ (0.33299)	47.74 52.26	0.6909 $(sp^{1.00})_C$ -0.7229 $(sp^{1.00})_C$	23.51
n_2 (O_7) (1.73654)			$\pi^*(C_4–C_5)$ (0.44281)	53.76 46.24	0.7332 $(sp^{1.00})_C$ -0.6800 $(sp^{1.00})_C$	29.73	$\pi^*(C_4–C_5)$ (0.43579)	54.20 45.80	0.7362 $(sp^{1.00})_C$ -0. 6768 $(sp^{1.00})_C$	30.61
			$\pi^*(C_8–O_{14})$ (0.28839)	69.54 30.46	0.8339 $(sp^{99.99})_C$ -0.5519 $(sp^{99.99})_O$	36.92	$\pi^*(C_8–O_{14})$ (0.25335)	68.02 31.98	0.8247 $(sp^{1.00})_C$ -0.5655 $(sp^{99.99})_O$	33.10
n_1 (N_{12}) (1.91480)			$\sigma^*(C_{11}–C_{15})$ (0.03096)	49.84 50.16	0.7060 $(sp^{1.86})_C$ - 0.7082$(sp^{2.17})_C$	11.28	$\sigma^*(C_{11}–C_{15})$ (0.03372)	50.54 49.46	0.7109 $(sp^{1.00})_C$ -0.7033 $(sp^{1.00})_C$	11.49
n_1 (N_{13}) (1.81940)			$\pi^*(C_{11}–N_{12})$ (0.21312)	56.94 43.06	0.7546 $(sp^{99.99})_C$ -0.6562 $(sp^{99.99})_N$	17.55	$\pi^*(C_{11}–N_{12})$ (0.21760)	55.54 44.46	0.7453 $(sp^{99.99})_C$ -0.6668 $(sp^{99.99})_N$	19.55
n_2 (O_{14}) (1.83275)			$\sigma^*(O_7–C_8)$ (0.12065)	29.63 70.37	0.5443 $(sp^{2.20})_O$ - 0.8389 $(sp^{2.98})_C$	38.49	$\sigma^*(O_7–C_8)$ (0.12498)	29.60 70.40	0.5440 $(sp^{2.25})_O$ - 0.8391 $(sp^{3.04})_C$	38.13
			$\sigma^*(C_8–C_9)$ (0.06804)	52.13 47.87	0.7220 $(sp^{1.44})_C$ - 0.6919 $(sp^{2.36})_C$	18.34	$\sigma^*(C_8–C_9)$ (0.07066)	52.18 47.82	0.7224 $(sp^{1.46})_C$ -0.6915 $(sp^{2.36})_C$	18.22
n_2 (O_{24}) (1.81479)			$\sigma^*(C_{16}–S_{23})$ (0.18647)	47.19 52.81	0.6869 $(sp^{3.28})_C$ - 0.7267 $(sp^{2.65})_S$	17.95	$\sigma^*(C_{16}–S_{23})$ (0.18309)	49.68 50.32	0.7048 $(sp^{3.57})_C$ -0.7094 $(sp^{2.68})_S$	16.74
							$\sigma^*(S_{23}–O_{25})$ (0.14526)	64.22 35.78	0.8014 $(sp^{2.57})_S$ -0.5982 $(sp^{3.16})_O$	11.21
n_3 (O_{24}) (1.80656)			$\sigma^*(N_{13}–S_{23})$ (0.28371)	36.20 63.80	0.6017 $(sp^{3.72})_N$ - 0.7988 $(sp^{3.92})_S$	20.46	$\sigma^*(N_{13}–S_{23})$ (0.28865)	36.92 63.08	0.6076 $(sp^{3.71})_N$ -0.7942 $(sp^{4.19})_S$	22.94
			$\sigma^*(S_{23}–O_{25})$ (0.16423)	66.84 33.16	0.8176 $(sp^{2.67})_S$ - 0.5758 $(sp^{2.86})_O$	13.78				
n_2 (O_{25}) (1.81799)			$\sigma^*(C_{16}–S_{23})$ (0.18647)	47.19 52.81	0.6869 $(sp^{3.28})_C$ - 0.7267 $(sp^{2.65})_S$	17.37	$\sigma^*(C_{16}–S_{23})$ (0.18309)	49.68 50.32	0.7048 $(sp^{3.57})_C$ -0.7094 $(sp^{2.68})_S$	16.91
n_3 (O_{25}) (1.77370)			$\sigma^*(N_{13}–S_{23})$ (0.28371)	36.20 63.80	0.6017 $(sp^{3.72})_N$ - 0.7988 $(sp^{3.92})_S$	21.89	$\sigma^*(N_{13}–S_{23})$ (0.28865)	36.92 63.08	0.6076 $(sp^{3.71})_N$ -0.7942 $(sp^{4.19})_S$	24.03
			$\sigma^*(S_{23}–O_{24})$ (0.14009)	66.53 33.47	0.8157 $(sp^{2.70})_S$ - 0.5785 $(sp^{2.89})_O$	16.22	$\sigma^*(S_{23}–O_{24})$ (0.13055)	64.14 35.86	0.8008 $(sp^{2.64})_S$ -0.5989 $(sp^{3.16})_O$	13.99

π(C9-C10)→π*(C8-O14) and π(O7)→π*(C4-C5) and (C8-O14) are responsible for conjugation of respective π-bonds in coumarin ring. The electron density at the conjugated π bonds (1.589–1.774) and π* bonds (0.422–0.200) of coumarin ring indicate strong π-electron delocalization within ring leading to a maximum stabilization of energy up to 36.92, 24.13, 20.53 Kcal/mol for B3LYP/6-31G(d,p) and B3LYP/6-311G(d,p) basis set. The interactions π(C18-C19)→π*(C20-C21) and π(C20-C21)→π*(C16-C17) are responsible for conjugation of respective π-bonds in tosyl ring. The electron density at the conjugated π bonds (1.623–1.654) and π* bonds (0.267–0.400) of tosyl ring indicate strong π-electron delocalization within

ring leading to a stabilization of energy in the range 17.53–18.34 kcal/mol. The interactions LP (N13)→π*(C11–N12), LP (O24)→π*(C16–S23) and π*(S23–O25) are respon-sible for conjugation of open chain structure. The respective electron density of π-bond on the N and O atom are (1.819–1.814) and π* bonds (0.164–0.213) indicate the strong electron delocalization in between azomethine group and sulphonyl group attached to tosyl ring with the energy of 13.78-17.95 Kcal/mol. The orbital overlap between bonding (π) and antibonding (π*) orbitals forms the charge transfer interactions. This leads to intramolecular charge transfer (ICT), which stabilizes the system. The intramolecular charge transfer (ICT), which is the transfer of π-electron cloud from donor to an acceptor, has the ability to increase a polarity of molecule and it is necessary for the molecule's NLO features. As a result, CHH compound may use for the non-linear optical materials applications.

Nonlinear optical properties (NLO): The first hyperpolarizability (β_0) and the related properties (*i.e.* dipole moment (μ_0), mean polarizability ($|\alpha_0|$), anisotropy of polarizability ($\Delta\alpha$)) [34,35] of CHH molecule were calculated at B3LYP/6–31G(d,p) and B3LYP/6–311G(d,p) basis set and are listed in Table-9. Significant charge delocalization is indicated by large values of specific polarizability and hyperpolarizability components. Since there were no experimental data available for the CHH molecule, *p*-nitroaniline (PNA) was selected as reference molecule in this investigation [36]. In PNA, a high value of polarizability (α) and hyperpolarizability (β_0) is caused by the intermolecular charge transfer combined with the existence of a suitable resonance structure. The values of first hyperpolarizability (β_0) for CHH were determined using the B3LYP/6–31G(d,p) and B3LYP/6–311G(d,p) basis set. In DMSO solvent, they were found to be 17.45×10^{-30} and 25.93×10^{-30} esu, respectively. These values are nearly half of the reference molecule (PNA, $\beta_0 = 50.27 \times 10^{-30}$ esu). Due to the transfer of the π-electron cloud from donor to acceptor, the CHH displays strong effective intramolecular charge transfer (ICT), high hyperpolarizability and potential significant non-linear optical properties in an optical field.

Chemical reactivity

Molecular electrostatic potential surface (MEPS) and global electronic descriptors: MEPS offer a way to visualize the relative polarity of a molecule. In addition, it is a helpful quantity in the explanation of hydrogen bonding, partial charges, the site of chemical reactivity, electronegativity and other molecular interactions, including those involving pharmaceuticals and biomolecules. Molecular electrostatic potential [V(r)] of a molecule is expressed by the following equation [37] given as:

$$V(r) = \sum_{a}^{Na} \frac{Z_A}{|r - R_A|} - \int \frac{\rho(r')d^3r'}{|r - r'|}$$

where Z_A represents the charge of nucleus A at R_A, Na represents the number of nuclei, and r' is a dummy integration variable. The effect of nuclei is represented by the first component in the formula, while the effect of electrons is represented by the second component. Due to their different signs, the two terms have opposing effects. Their resultant, V(r), is an indication of the net electrostatic impact generated at each position r by the molecule's overall charge distribution (electron + nuclei).

In addition to being a highly helpful descriptor for identifying places for electrophilic attack and nucleophilic reactions, the molecule electrostatic potential is also correlated with the electron density [38]. To predict electrophilic and nucleophilic reactive sites for CHH, the MEPS map calculated at B3LYP/6-311G(d,p) basis set is shown in Fig. 7. The different values of the electrostatic potential at the surface are represented by different colours. Potential increases in the order red < orange < yellow < green < blue. The negative (red, orange and yellow) regions of the MEP are related to the electrophilic reactivity. The maximum positive region is localized around the hydrogen atoms attached to the nitrogen atom of azomethine (HC=NNH) frame, indicating a possible site for nucleophilic attack. The MEPS map (Fig. 7) shows that the negative potential sites are on electronegative O atom.

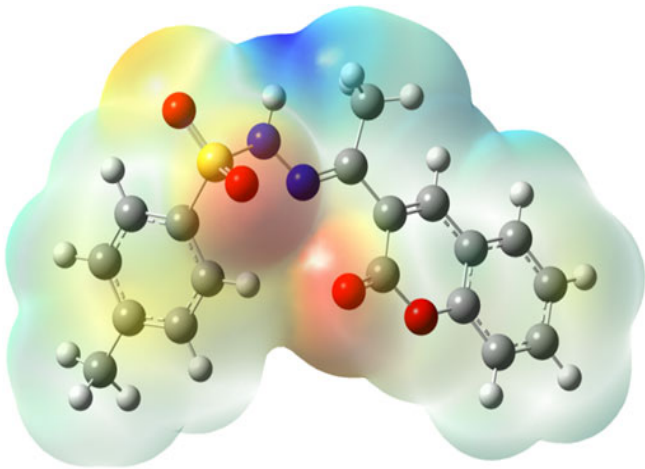

Fig. 7. Molecular electrostatic potential surface (MEPS) map for CHH

Koopman's theorem [39,40] has been used to determine the chemical reactivity and site selectivity. Global reactivity trends [40] can be highly accurately predicted by electronegativity (χ) = $-1/2(\varepsilon_{LUMO} + \varepsilon_{HOMO})$, chemical potential ($\mu$) = $1/2(\varepsilon_{LUMO} + \varepsilon_{HOMO})$, global softness (S) = $1/2\eta$, global hardness (η) = 1/2

TABLE-9
CALCULATED DIPOLE MOMENT (μ), POLARIZABILITY ($|\alpha_0|$), ANISOTROPY OF POLARIZABILITY ($\Delta\alpha$), FIRST HYPERPOLARIZABILITY (β_0) AT B3LYP/6–31G(d,p)/B3LYP/6–311G(d,p) FOR CHH IN DMSO SOLVENT

Basis set	μ	α_0	$\Delta\alpha$	β_0
6–31G(d,p) CHH	7.491	29.376	52.842	17.450
6–311G(d,p) CHH	11.634	38.371	70.985	25.900
6–31G(d,p) PNA	9.898	17.086	28.417	50.275
6–311G(d,p) PNA	9.337	16.660	27.248	44.069

($\varepsilon_{LUMO} - \varepsilon_{HOMO}$) and global electrophilicity index ($\omega = \mu^2/2\eta$ descriptors for (**1**), (**2**), (**3**) and ECT for reactant system [(**1**)→(**2**)] are listed in Table-10. The global electrophilicity index (ω = 4.89 eV) for CHH shows that it behaves as a strong electrophile. The ΔN reactivity index quantifies the energy stabilization that takes place when the system absorbs an additional electronic charge (ΔN) from its environment. The direction of the charge transfer is completely determined by the molecule's electronic chemical potential since an electrophile is a chemical species that may accept electrons from its surroundings and whose energy must decrease upon obtaining electronic charge. This means that its electrical chemical potential must be negative.

TABLE-10
CALCULATED GLOBAL ELECTRONIC DESCRIPTORS OF INVESTIGATED MOLECULE CHH AT B3LYP/6-311G(d,p) BASIS SET

Global parameter	(1)	(2)	(3)
HOMO (E_H)	-6.9224	-7.1676	-6.3641
LUMO (E_L)	-2.6625	-1.1825	-2.4231
Electronegativity (χ)	4.8075	4.1751	4.3936
Chemical potential (μ)	-4.8075	-4.1751	-4.3936
Electrophilicity index (ω)	5.4639	2.9125	4.8982
Softness (S)	0.2364	0.1670	0.2537
Hardness (η)	2.1149	2.9925	1.9704
ECT			-0.88

Electrophilic charge transfer (ECT) = $(\Delta N_{max})_A - (\Delta N_{max})_B$ [39] is defined as the difference between the ΔN_{max} values of interacting molecules. If we consider two molecules A and B approach to each other (i) if ECT > 0, charge flow from B to A (ii) if ECT < 0, charge flow from A to B. ECT is calculated as -0.88 *i.e.* ECT < 0 for reactant system [(**1**)→(**2**)], which indicates that charge flows from (**2**) to (**1**). Therefore, (**1**) acts as electron acceptor (electrophile) and (**2**) as electron donor (nucleophile). The high value of elecrophilicity index for (**1**) than (**2**) also favours electrophilic behaviour of (**1**) and nucleophilic behaviour of (**2**). The electronegativity of (**1**) is higher as compared to (**2**), which again indicate that charge flow from (**2**) to (**1**).

Theoretical biological investigations

ADMET studies: Several potential drugs have been shelved due to unpleasant side effects and insufficient drug-like properties, either during the drug research process or during clinical trials. The effect of the geometrical and structural properties on the bioavailability of CHH can be better visualized considering the bioavailability radars as displayed in Fig. 8. The pink area represents the optimal range for each property which is lipophilicity, size, polarity, solubility, saturation and flexibility. While the bioactivity of CHH towards the different targets is considered to be good, its interactions as a G-protein coupled receptor (GPCR) ligand and protease inhibitors could be an important for its consideration as a potential therapeutic drug. The optimized CHH, acetyl coumarin and *p*-toluene sulphonylhydrazide were evaluated for drug-relevant characteristics and toxicity risks to determine the drug-like properties, the lead compounds represent. The CHH, acetyl coumarin and *p*-toluene sulphonylhydrazide may be able to inhibit the cancer osaka thyroid kinase caco-2, according to ADME investigation [41]. Acetyl coumarin showed high human intestinal absorption (HIA) values of 98.03% as compared to CHH and *p*-toluene sulphonylhydrazide suggesting that oral administration might improve intestinal absorption. A value close to 1.00 for the blood brain barrier (BBB) indicates that a drug is able to permeate the CNS with relative ease [42]. The cytochrome P-450 (CYP-450) enzymes are mostly expressed in the liver; however they are also present in the small intestine, lungs, placenta and kidney. The isozymes CYP2D6, CYP2C19 and CYP2C9 are involved in the hepatic metabolism of numerous medications containing amine functional groups [43,44]. The results of the inhibition and substrate activity of above mentioned CYP-450 enzymes and the plasma protein binding activity of CHH, acetyl coumarin and *p*-toluene sulphonylhydrazide are shown in Table-11. The ADME results of CHH, acetyl coumarin and *p*-toluene sulphonylhydrazide shows that they all may be the inhibitors of CYP-2C19 isozyme of P-450 coenzyme and were found low bounded to plasma protein *i.e.* 88.87, 74.97, 45.82%, respectively. All CHH, acetyl coumarin and *p*-toluene

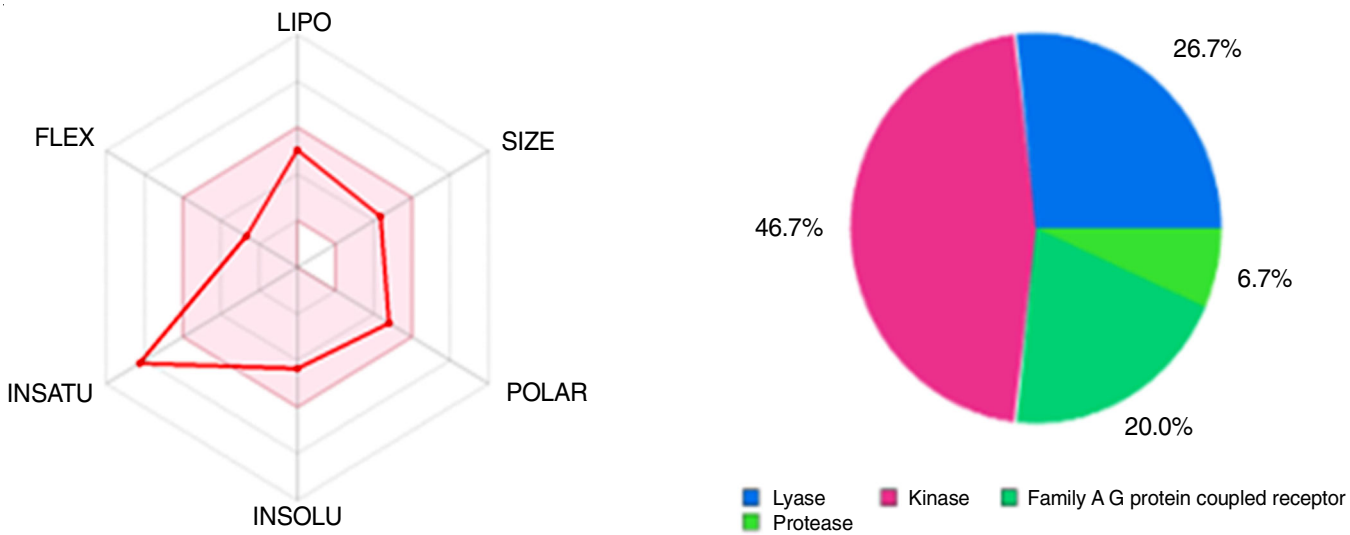

Fig. 8. Bioavailability radars and predicted biological targets of coumarin based hydrazide-hydrazone (CHH) derivative

TABLE-11
CALCULATED ADME AND PRE-ADMET PREDICTION OF CHH

ID	CHH	Acetyl coumarin	*p*-Toluene sulphonylhydrazide
BBB	0.7513	1.5487	0.4035
Caco2	3.2749	21.7004	0.3641
CYP-2C19-inhibition	Inhibitor	Inhibitor	No
CYP-2C9-inhibition	Inhibitor	Inhibitor	Inhibitor
CYP-2D6-inhibition	No	No	No
CYP-2D6-substrate	No	No	No
HIA	96.351804	98.0362	91.1509
MDCK	1.0191	47.4972	7.3102
Pgp-inhibition	No	No	No
Plasma-Protein-Binding	88.8684	74.9785	45.8292
GI absorption	High	High	High

sulphonylhydrazide compounds satisfy Lipinski's rule [45], as evidenced by the molecular weight of CHH, which is 356.40, 188.18 and 186.23 g/mol, respectively, which is less than 500 g/mol, the LogP and hydrogen bond donor (HBD) values being less than 5 and the hydrogen bond acceptor (HBA) values for all being less than 10. The CHH, acetyl coumarin and *p*-toluene sulphonylhydrazide exhibit strong oral absorption in computer computations as a result. The calculated topological polar surface area (TPSA) value for CHH and *p*-toluene sulphonylhydrazide was found 97.12 and 80.57 Å, respectively, which are less than 140 Å indicate high permeability, absorption and transport *via* biological membranes. The synthesized molecule CHH has good synthetic feasibility, as indicated by the bioavailability score of 0.55, the drug-likeness model and the expected pharmacological features.

***In silico* study:** An effective way to investigate the characteristics of protein-ligand interactions and validate the biological activity inside any chemical structure is through molecular docking studies [46]. PYMOL software was used to visualize protein-ligand interaction [47].

Anti-HIV activity: The current study makes use of the crystal structure of the unmutated common ancestor (UCA) with PDB ID 6p3b, the anti-HIV antibody DH501. Fig. 9a displays a Ramachandran plot (RC), which is used to examine the interaction characteristics of proteins [48]. The stability of the proteins selected for docking simulation is indicated by the (RC) plot, where distinct colour sections represent the residues in the most favoured region, allowed region and generously allowed region. The (RC) uses blue dots to represent the protein structure in each of the plot's regions. "Boxed" regions were filled with red (core), brown (allowed) and yellow (generously allowed) [49]. The 50% region is indicated by the inner lines, while the outside lines surround the area that should contain 90% of all dots of the same colour. The majority of the amino acid residues in both proteins are located in their permitted regions.

Protein ligand interactions and H bond interactions for CHH is shown in Fig. 9b. The HIV protein residues interacted with the synthesized CHH, including THR′31, GLY′32, ARG′100, ARG′96, ILE′100, ASP′100, THR′100, TYR′32, LEU′89, TRP′96, TYR′58, TYR′31 and TYR′91 with various interactions. The docking results indicate the CHH has a strong binding affinity for anti-HIV antibody DH501, suggesting that the anti-HIV protein is well-docked. The CHH compound has

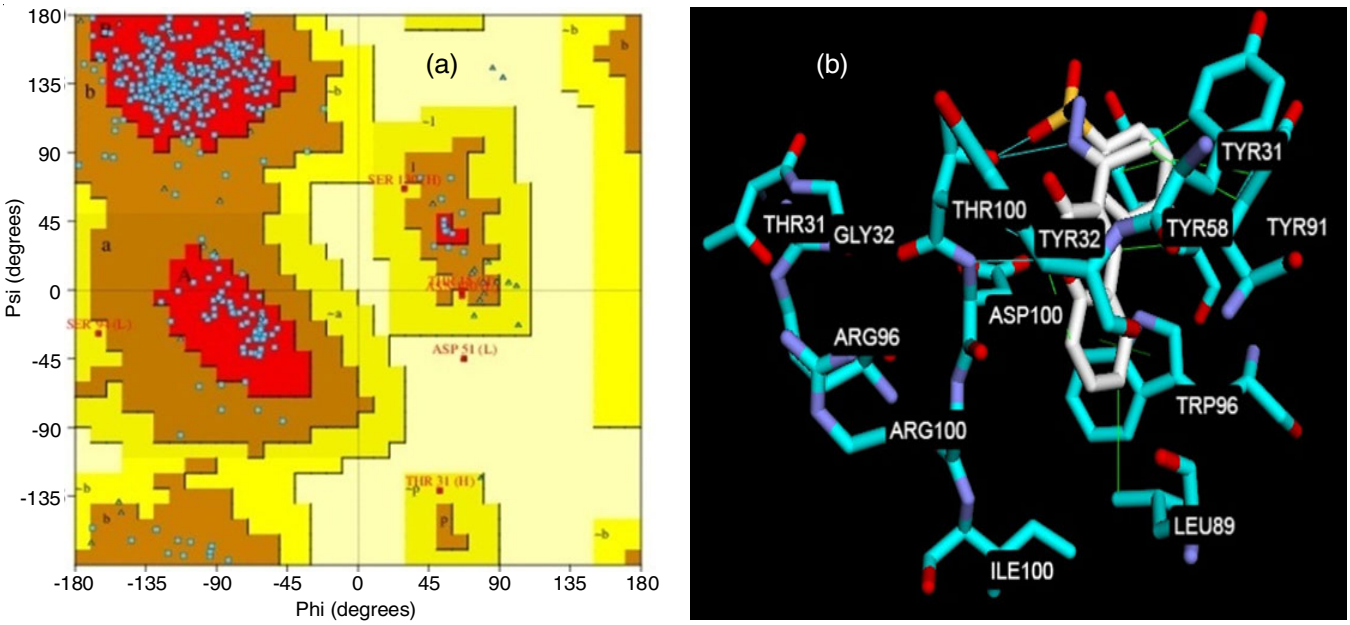

Fig. 9. (a) Ramachandran plot for 6p3b protein structure of anti-HIV antibody DH501, (b) protein ligand interaction images/H bond interaction

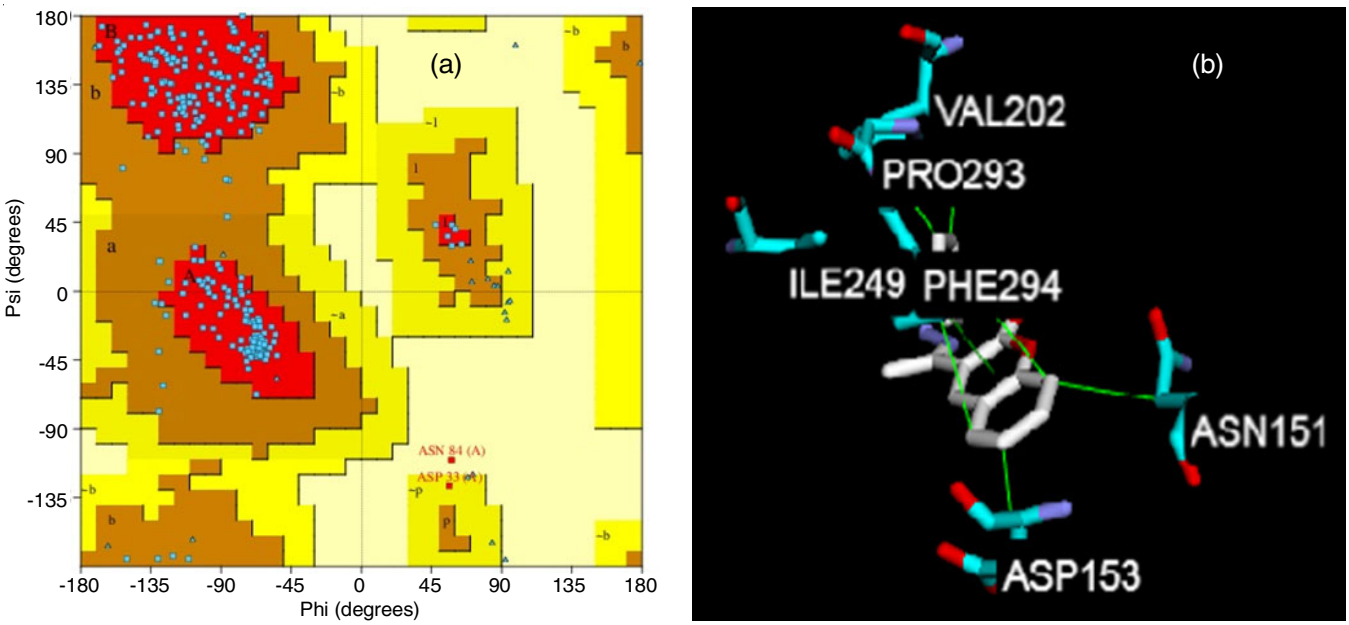

Fig. 10. (a) Ramachandran plot for 6lu7 protein structure of COVID-19 main protease, (b) protein ligand interaction images/H bond interaction

favourable interactions and characteristics with the receptor molecules, according to the results of a molecular docking and it is anticipated to be a promising anti-HIV medicine or agent.

Anti-SARS-CoV-2 activity: The Ramachandran plot of 6lu7 protein structure of COVID-19 major protease and the protein ligand interactions of CHH with M^{pro} SARS-CoV-2 protein is shown in Fig. 10. The CHH have a strong binding affinity for 6lu7, having -7.80 Kcal/mol binding energy, suggesting that the anti-SARS-CoV-2 protein is properly docked with the CHH ligand. The investigated compound CHH interacted with various residues of the SARS-CoV-2 proteins, specifically ASP′153, VAL′202, PRO′293, PHE′294, ILE′249 and ASN′151. The CHH compound has favourable interactions and characteristics with the receptor molecules, according to the results of a molecular docking research and it is anticipated to be a viable anti-SARS-CoV-2 medication or agent.

Conclusion

Using the basis sets B3LYP/6-31G(d,p) and B3LYP/6-311G-(d,p), the coumarin hydrazide-hydrazone derivative (CHH) has been synthesized and computed by combined experimental and theoretical results. A significant increase in yield and reduction in reaction time have been observed in the grinding procedure when compared to conventional method. The rotational barrier has also been studied at B3LYP/6-311G(d,p) basis set and the rotational barrier between conformer I and conformer II of CHH was found 5.102 Kcal/mol in the gas phase. The NBO analysis investigation indicates the various types of interactions within molecule. Topological parameters have been analyzed by Bader's 'atoms in molecules' AIM theory and provide the existence of intramolecular interactions such as hydrogen-hydrogen (H---H) and oxygen-nitrogen (O---N) interaction. The first hyperpolarizability (β_0) of CHH was found to be as 25.93×10^{-30} esu at B3LYP/6-311G(d,p) indicates that CHH may be suitable for NLO applications. The molecular docking results suggested that the CHH compound exhibits relatively good antiviral activity targeted against SARS COV-2 major protein (M^{pro}) with PDB code 6lu7 and anti-HIV antibody DH501, an unmutated common ancestor with PDB ID 6p3b. By comparing calculated and experimental results of electronic transitions, chemical shifts and wavenumbers it have been observed that B3LYP/6-311G(d,p) estimated better results.

ACKNOWLEDGEMENTS

The authors sincerely thank the Department of Chemistry, University of Lucknow, Lucknow, India for the spectral analysis facilities and infrastructure provided for the research work. The authors are also thankful to the CSIR, New Delhi for providing research fund.

CONFLICT OF INTEREST

The authors declare that there is no conflict of interests regarding the publication of this article.

REFERENCES

1. D.J. Newman and G.M. Cragg, *J. Nat. Prod.*, **83**, 770 (2020); https://doi.org/10.1021/acs.jnatprod.9b01285
2. Q.C. Ren, C. Gao, Z. Xu, L.S. Feng, M.L. Liu, X. Wu and F. Zhao, *Curr. Top. Med. Chem.*, **18**, 101 (2018); https://doi.org/10.2174/1568026618666180221114515
3. T. Abe, Y. Marutani and I. Shoji, *Microbiol. Immunol.*, **63**, 51 (2019); https://doi.org/10.1111/1348-0421.12669
4. Y. Hu, W. Chen, Y. Shen, B. Zhu and G.X. Wang, *Bioorg. Med. Chem. Lett.*, **29**, 1749 (2019); https://doi.org/10.1016/j.bmcl.2019.05.019
5. T.M. Khomenko, V.V. Zarubaev, I.R. Orshanskaya, R.A. Kadyrova, V.A. Sannikova, D.V. Korchagina, K.P. Volcho and N.F. Salakhutdinov, *Bioorg. Med. Chem. Lett.*, **27**, 2920 (2017); https://doi.org/10.1016/j.bmcl.2017.04.091
6. L. De Luca, F.E. Agharbaoui, R. Gitto, M.R. Buemi, F. Christ, Z. Debyser and S. Ferro, *Mol. Inform.*, **35**, 460 (2016); https://doi.org/10.1002/minf.201501034

7. T.O. Olomola, R. Klein, N. Mautsa, Y. Sayed and P.T. Kaye, *Bioorg. Med. Chem.*, **21**, 1964 (2013); https://doi.org/10.1016/j.bmc.2013.01.025
8. P. Zhou, Y. Takaishi, H. Duan, B. Chen, G. Honda, M. Itoh, Y. Takeda, O.K. Kodzhimatov and K.H. Lee, *Phytochemistry*, **51**, 781 (2000); https://doi.org/10.1016/S0031-9422(99)00554-3
9. C.I. Paules, H.D. Marston and A.S. Fauci, *JAMA*, **323**, 707 (2020); https://doi.org/10.1001/jama.2020.0757
10. S. Mishra, A. Pandey and S. Manvati, *Heliyon*, **6**, e03217 (2020); https://doi.org/10.1016/j.heliyon.2020.e03217
11. M.Z. Hassan, H. Osman, M.A. Ali and M.J. Ahsan, *Eur. J. Med. Chem.*, **123**, 236 (2016); https://doi.org/10.1016/j.ejmech.2016.07.056
12. K.N. Venugopala, V. Rashmi and B. Odhav, *BioMed Res. Int.*, **2013**, 963248 (2013); https://doi.org/10.1155/2013/963248
13. Y. Shikishima, Y. Takaishi, G. Honda, Y. Takeda, O.K. Kodzhimatov, M. Ito, O. Ashurmetov and K.H. Lee, *Chem. Pharm. Bull.*, **49**, 877 (2001); https://doi.org/10.1248/cpb.49.877
14. N. Márquez, R. Sancho, L.M. Bedoya, J. Alcamí, J.L. López-Pérez, A. San Feliciano, B.L. Fiebich and E. Muñoz, *Antivir. Res.*, **66**, 137 (2005); doi.org/10.1016/j.antiviral. 2005. 02.006
15. N.F. Holguín, J. Frau and D.G. Mitnik, *Front Chem.*, (2021); https://doi.org/10.3389/fchem.2021.708364
16. S. Yadav, S. Singh and C. Gupta, *Curr. Res. Green Sust. Chem.*, **5**, 100260 (2022); https://doi.org/10.1016/j.crgsc.2022.100260
17. M. Molnar, M. Lonèariæ and M. Kovaè, *Curr. Org. Chem.*, **24**, 4 (2020); https://doi.org/10.2174/1385272824666200120144305
18. M.J. Frisch, G.W. Trucks, H.B. Schlegel, G.E. Scuseria, M.A. Robb, J.R. Cheeseman, G. Scalmani, V. Barone, G.A. Petersson, H. Nakatsuji, X. Li, M. Caricato, A.V. Marenich, J. Bloino, B.G. Janesko, R. Gomperts, B. Mennucci, H.P. Hratchian, J.V. Ortiz, A.F. Izmaylov, J.L. Sonnenberg, D. Williams-Young, F. Ding, F. Lipparini, F. Egidi, J. Goings, B. Peng, A. Petrone, T. Henderson, D. Ranasinghe, V.G. Zakrzewski, J. Gao, N. Rega, G. Zheng, W. Liang, M. Hada, M. Ehara, K. Toyota, R. Fukuda, J. Hasegawa, M. Ishida, T. Nakajima, Y. Honda, O. Kitao, H. Nakai, T. Vreven, K. Throssell, J.A. Montgomery Jr., J.E. Peralta, F. Ogliaro, M.J. Bearpark, J.J. Heyd, E.N. Brothers, K.N. Kudin, V.N. Staroverov, T.A. Keith, R. Kobayashi, J. Normand, K. Raghavachari, A.P. Rendell, J.C. Burant, S.S. Iyengar, J. Tomasi, M. Cossi, J.M. Millam, M. Klene, C. Adamo, R. Cammi, J.W. Ochterski, R.L. Martin, K. Morokuma, O. Farkas, J.B. Foresman and D.J. Fox, Gaussian, Inc. Wallingford CT (2010).
19. A.D. Becke, *J. Chem. Phys.*, **98**, 5648 (1993); https://doi.org/10.1063/1.464913
20. C.T. Lee, W.T. Yang and R.G.B. Parr, *Phys. Rev. B Condens. Matter*, **37**, 785 (1988); https://doi.org/10.1103/PhysRevB.37.785
21. G.A. Petersson and M.A. Al-laham, *J. Chem. Phys.*, **94**, 6081 (1991); https://doi.org/10.1063/1.460447
22. G.A. Petersson, A. Bennett, T.G. Tensfeldt, M.A. AlLaham, W.A. Shirley and J. Mantzaris, *J. Chem. Phys.*, **89**, 2193 (1988); https://doi.org/10.1063/1.455064
23. K.C. Mariamma, H.T. Varghese, C.Y. Panicker, K. John, J. Vinsova and C. Van Alsenoy, *Spectrochim. Acta A Mol. Biomol. Spectrosc.*, **112**, 161 (2013); https://doi.org/10.1016/j.saa.2013.04.052
24. K.N. Chethan Prathap and N.K. Lokanath, *J. Mol. Struct.*, **1158**, 26 (2018); https://doi.org/10.1016/j.molstruc.2018.01.007
25. A.P. Scott and L. Radom, *J. Phys. Chem.*, **100**, 16502 (1996); https://doi.org/10.1021/jp960976r
26. NIST Computational Chemistry Comparison and Benchmark Database NIST Standard Reference Database Number 101, Russell D. Johnson III (2022); https://doi.org/10.18434/T47C7Z
27. R. Alphonse, A. Varghese, L. George and A. Nizam, *J. Mol. Liq.*, **215**, 387 (2016); https://doi.org/10.1016/j.molliq.2015.12.050
28. R.G. Pearson, Chemical Hardness: Applications from Molecules to Solids Wiley- VCH, Weinheim, Germany (1997).
29. R.E. Aderne, B.G.A.L. Borges, H.C. Ávila, F. von Kieseritzky, J. Hellberg, M. Koehler, M. Cremona, L.S. Roman, C.M. Araujo, M.L.M. Rocco and C.F.N. Marchiori, *Mater. Adv.*, **3**, 1791 (2022); https://doi.org/10.1039/D1MA00652E
30. M. Snehalatha, C. Ravikumar, I. Hubert Joe, N. Sekar and V.S. Jayakumar, *Spectrochim. Acta A Mol. Biomol. Spectrosc.*, **72**, 654 (2009); https://doi.org/10.1016/j.saa.2008.11.017
31. D.W. Schwenke and D.G. Truhlar, *J. Chem. Phys.*, **82**, 2418 (1985); https://doi.org/10.1063/1.448335
32. M. Gutowski, J.G.C.M. Van Duijneveldt-Van de Rijdt, J.H. Van Lenthe and F.B. Van Duijneveldt, *J. Chem. Phys.*, **98**, 4728 (1993); https://doi.org/10.1063/1.465106
33. F. Weinhold, C.R. Landis and E.D. Glendening, *Int. Rev. Phys. Chem.*, **35**, 399 (2016); https://doi.org/10.1080/0144235X.2016.1192262
34. D.A. Kleinman, *Phys. Rev.*, **126**, 1977 (1962); https://doi.org/10.1103/PhysRev.126.1977
35. H. Alyar, Z. Kantarci, M. Bahat and E. Kasap, *J. Mol. Struct.*, **834-836**, 516 (2007); https://doi.org/10.1016/j.molstruc.2006.11.066
36. J.L. Oudar and D.S. Chemla, *J. Chem. Phys.*, **66**, 2664 (1977); https://doi.org/10.1063/1.434213
37. N. Sukumar, A Matter of Density: Exploring the Electron Density Concept in the Chemical, Biological, and Materials Sciences, Wiley-Blackwell (2012).
38. P. Rawat and R.N. Singh, *Spectrochim. Acta A Mol. Biomol. Spectrosc.*, **140**, 344 (2015); https://doi.org/10.1016/j.saa.2014.12.080
39. R.G. Parr, L. Szentpály and S. Liu, *J. Am. Chem. Soc.*, **121**, 1922 (1999); https://doi.org/10.1021/ja983494x
40. R.G. Parr and W. Yang, Density Functional Theory of Atoms and Molecules, Oxford University Press, New York (1989).
41. A. Daina, O. Michielin and V. Zoete, *Sci. Rep.*, **7**, 42717 (2017); https://doi.org/10.1038/srep42717
42. M. Alsawalha, S.R. Bolla, N. Kandakatla, V. Srinivasadesikan, V.P. Veeraraghavan and K.M. Surapaneni, *Bioinform.*, **15**, 380 (2019); https://doi.org/10.6026/97320630015380
43. R. Yuan, S. Madani, X.X. Wei, K. Reynolds and S.M. Huang, *Drug Metab. Dispos.*, **30**, 1311 (2002); https://doi.org/10.1124/dmd.30.12.1311
44. J.E. McGraw, A Handbook of Pharmacogenomics and Stratified Medicine, Elsevier Publication (2014).
45. F. Cheng, W. Li, Y. Zhou, J. Shen, Z. Wu, G. Liu, P.W. Lee and Y.T. Admet, *J. Chem. Inf. Mod.*, **52**, 3099 (2012); https://doi.org/10.1021/ci300367a
46. M.M. Julie, T. Prabhu, E. Elamuruguporchelvi, F.B. Asif, S. Muthu and A. Irfan, *J. Mol. Liq.*, **336**, 116335 (2021); https://doi.org/10.1016/j.molliq.2021.116335
47. L. Schrödinger and W. DeLano, *PyMOL.* 2020; http://www.pymol.org/pymol
48. https://www.ebi.ac.uk/thornton-srv/databases/pdbsum/
49. A.T. Dubis, S.J. Grabowski, D.B. Romanowska, T. Misiaszek and J. Leszczynski, *J. Phys. Chem. A*, **106**, 10613 (2002); https://doi.org/10.1021/jp0211786